==================== MATHEMATICAL MODELING ====================

Computational Modeling Analysis of Acute and Chronic Ethanol-Induced Oxidative Stress

Markevich N.I.[1,2*], Hoek J.B.[1]

[1]*Department of Pathology, Anatomy, and Cell Biology, Thomas Jefferson University, Philadelphia, PA 19107, USA*
[2]*Institute of Theoretical and Experimental Biophysics RAS, Pushchino, 142290, Russia*

Abstract. The main goal of this work is to develop a computational model of reactive oxygen species (ROS) production by the mitochondrial respiratory chain and analyze the control of oxidative stress that is enhanced by acute and excessive chronic ethanol treatment, resulting in ethanol-induced injury. The computational model consists of a system of 35 ordinary differential equations and describes the oxidized and reduced states of different electron carriers and the electron flow through Complexes I, II, III and IV as well as the rates of superoxide and H_2O_2 production and degradation in the control and upon ethanol-related alterations in different segments of the respiratory chain and glutathione peroxidase and glutathione reductase reactions. The effect of acute ethanol metabolism on ROS production was simulated in the computational model by an increase in the mitochondrial NADH/NAD ratio and a closure of voltage dependent anionic channel (VDAC) in the outer mitochondrial membrane. Excessive chronic ethanol consumption was modeled in accord with experimental observations available in the literature through inhibition of the activity of different segments of the respiratory chain and glutathione peroxidase as well as activation of glutathione reductase and changes in the total mitochondrial glutathione levels. Computational analysis of $\Delta\Psi$ dependencies of ROS production upon chronic ethanol consumption during oxidation of different respiratory substrates was carried out. Computational results show that chronic ethanol increases the concentration of superoxide and H_2O_2 in the mitochondrial matrix over the entire range of the membrane potential of $0 < \Delta\Psi < 180$ mV during oxidation of NADH alone and NADH + succinate. Ethanol-induced changes in the concentration of superoxide in the intermembrane space (IMS) are non-monotonic and depend on the membrane potential under this condition due to non-monotonic alterations in the rate of superoxide generation by the unstable semiquinone of Complex III. Ethanol-induced alterations in the concentration of both superoxide and H_2O_2 in the mitochondrial matrix and IMS are also non-monotonic and depend on $\Delta\Psi$ during oxidation of succinate alone. Computational results are very compatible with available experimental observations of ROS production under control condition and acute and chronic ethanol treatment and predict that the effect of ethanol on ROS production depends on the membrane potential, i.e. metabolic state of mitochondria.

Keywords: reactive oxygen species (ROS), mitochondrial respiratory chain, computational model, acute and chronic alcohol.

INTRODUCTION

Mitochondria are the major intracellular source of re active oxygen species (ROS) and they are recognized as an important target for damaging effects of ethanol [1–3]. The main sites of formation of reactive oxygen in mitochondria are complexes I and III of the

---

*markevich.nick@gmail.com

mitochondrial respiratory chain. Complex I-generated superoxide is vectorially released into the mitochondrial matrix while Complex III releases superoxide to both sides of the inner mitochondrial membrane [4].

Acute ethanol exposure increases ROS production by both Complexes I and III due to generation of excess of cytosolic NADH resulting from alcohol dehydrogenase reaction [5–7]. Cytosolic NADH is oxidized indirectly by mitochondrial NADH dehydrogenase (Complex I) which depends on the malate-aspartate shuttle in the inner mitochondrial membrane [8]. Another important ethanol dependent process that controls oxidative stress to the cytosol is a release of superoxide and hydrogen peroxide H_2O_2 through VDAC located in the outer mitochondrial membrane. It was demonstrated recently [9] that acute ethanol exposure decreases mitochondrial outer membrane permeability, which is very likely due to inhibition of VDAC. This inhibition results in additional acute ethanol-induced increase in the ROS level in mitochondria because of a decrease in efflux of ROS to the cytosol through VDAC.

Chronic ethanol treatment can also increase mitochondrial ROS production due to depression of the activity of different segments of the respiratory chain and inhibition of glutathione peroxidase reaction [1, 10, 11]. Chronic ethanol-induced activation of ROS generation occurs via multiple structural changes in the individual components of the respiratory chain resulting in inhibition of its activity [12]. Electron transfer through Complex I is reduced due to a decrease in the content of iron-sulfur centers of Complex I in mitochondria from ethanol-fed animals [13]. Chronic ethanol consumption also decreases the cyt b content in Complex III [14] as well as the activity of cytochrome c oxidase [14, 15]. Chronic ethanol-induced inhibition of ROS degradation in glutathione peroxidase reaction occurs via inhibition of the activity of glutathione peroxidase and changes in the mitochondrial glutathione level [11, 16].

These experimental observations show very complex alterations in mitochondria associated with acute and chronic excessive ethanol consumption. The effect of these alterations on the rate of ROS generation in the respiratory chain and steady-state concentration of mitochondrial ROS within the mitochondrial matrix and intermembrane space (IMS) is difficult to predict when based just on experimental studies. It requires a computational modeling analysis which takes into account ethanol-induced alterations in both processes of ROS generation and degradation. Cadenas and Devies [17] reviewed earlier the mitochondrial rates of ROS production and degradation and steady state levels of the mitochondrial concentration of superoxide and H_2O_2 in the absence of alcohol treatment.

In this work, we analyzed quantitatively alterations in the steady state of mitochondrial ROS production and degradation upon acute and chronic ethanol treatment with the help a computational model taking into account ethanol-induced alterations in different parts of mitochondrial ROS metabolism.

METHODS AND MODELS

1. Schematic kinetic model of the respiratory chain

A kinetic scheme of electron transfer and production of superoxide anion and hydrogen peroxide H_2O_2 underlying a mechanistic computational model of the mitochondrial respiratory chain is presented in Fig. 1. This simplified kinetic scheme includes the following electron carriers: a) for Complex I (NADH dehydrogenase, also called NADH:Ubiquinone Oxidoreductase), flavine mononucleotide (FMN), the sequence of iron-sulfur clusters beginning N3 and N1a and ending N2 cluster, and coenzyme Q; b) for Complex III (Cytochrome bc1 complex, also called Ubiquinol:Cytochrome c Oxidoreductase), coenzyme Q, non-heme iron-sulfur protein (ISP), cytochromes bL, bH and c1; c) Cytochrome c and d) Cytochrome c oxidase, also known as Complex IV. Complex II (Succinate dehydrogenase) and Complex IV are taken as the total complexes, since Complexes II and IV are not direct

sources of ROS during mitochondrial electron transport. Electron transfer in Complexes I and III were described in detail to take into account electron carrier states responsible for bypass reduction of O_2 resulting in superoxide formation. These bypass reactions are marked by red arrows in the kinetic scheme (Fig. 1).
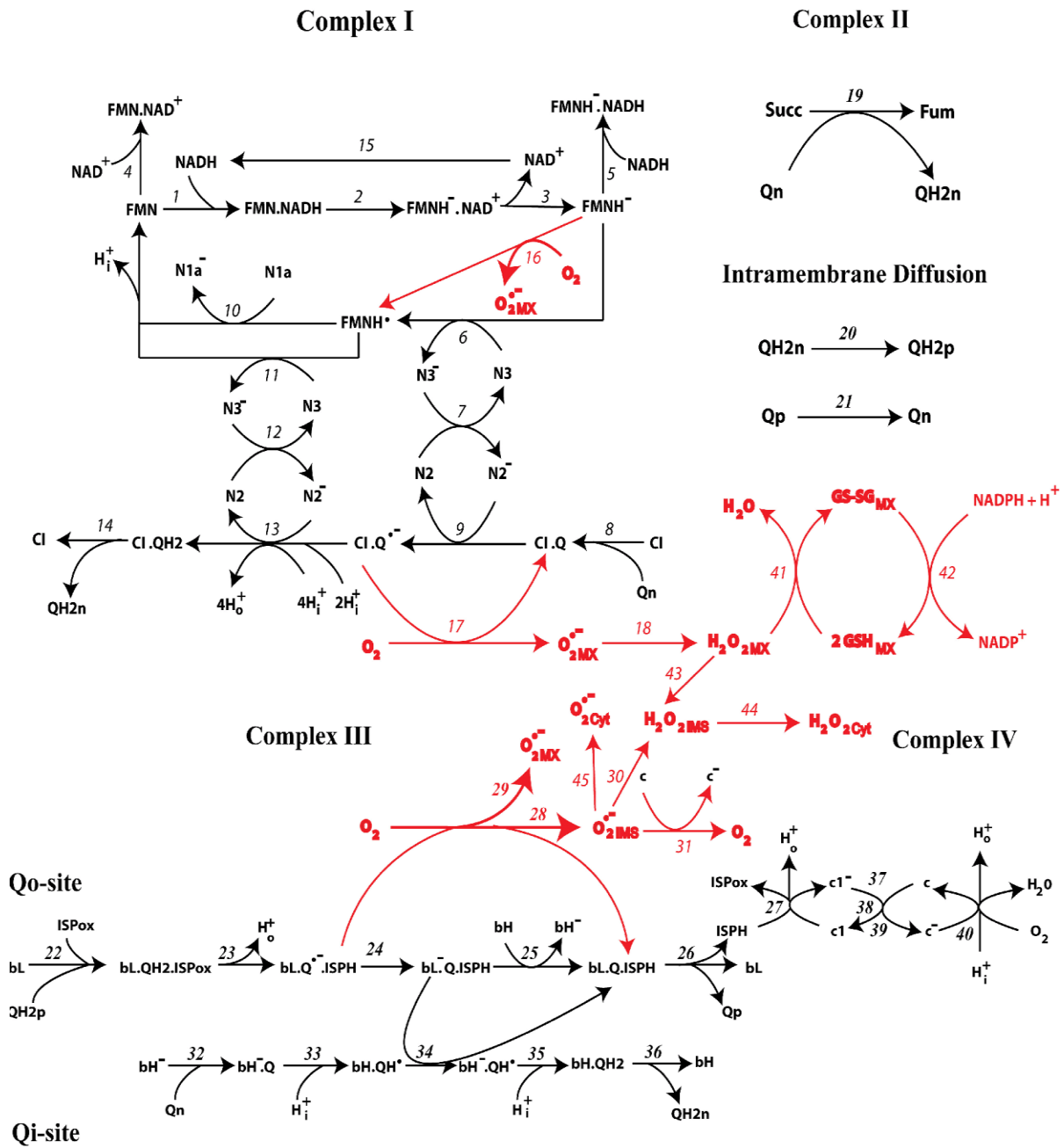

Figure 1. Kinetic scheme of electron transfer in the respiratory chain and reactions of superoxide and hydrogen peroxide H_2O_2 production and utilization. Reactions of superoxide and H_2O_2 formation and utilization are shown by red arrows. Detailed reaction network is presented in Table 1.

The entire reaction network of electron transfer and ROS production and degradation corresponding to the kinetic scheme in Fig. 1 consists of 45 reaction rates which are described in detail in Table 1.

65

Table 1. Chemical and rate equations in the model of respiratory chain

No	Reaction	Rate equation
Electron transfer in Complex I		
1	NADH + FMN = FMN.NADH	$V_1 = k_1 \cdot$ (NADH $\cdot$ FMN – FMN.NADH/K_{eq1})
2	FMN.NADH = FMNH⁻.NAD⁺	$V_2 = k_2 \cdot$ (FMN.NADH – FMNH⁻.NAD⁺/K_{eq2})
3	FMNH⁻.NAD⁺ = FMNH⁻ + NAD⁺	$V_3 = k_3 \cdot$ (FMNH⁻.NAD⁺ – FMNH⁻ $\cdot$ NAD⁺/K_{eq3})
4	FMN + NAD⁺ = FMN.NAD⁺	$V_4 = k_4 \cdot$ (FMN $\cdot$ NAD⁺ – FMN.NAD⁺/K_{eq4})
5	FMNH⁻ + NADH = FMNH⁻.NADH	$V_5 = k_5 \cdot$ (FMNH⁻ $\cdot$ NADH – FMNH⁻.NADH/K_{eq5})
The first electron transfer		
6	FMNH⁻ + N3 = FMNH· + N3⁻	$V_6 = k_6 \cdot$ (FMNH⁻ $\cdot$ N3 – FMNH· $\cdot$ N3⁻/K_{eq6})
7	N3⁻ + N2 = N3 + N2⁻	$V_7 = k_7 \cdot$ (N3⁻ $\cdot$ N2 – N3 $\cdot$ N2⁻/K_{eq7})
8	CI + Qn = CI.Q	$V_8 = k_8 \cdot$ (CI $\cdot$ Qn – CI.Q/K_{eq8})
9	CI.Q + N2⁻ = CI.Q·⁻ + N2	$V_9 = k_9 \cdot$ (CI.Q $\cdot$ N2⁻ – CI.Q·⁻ $\cdot$ N2/K_{eq9})
The second electron transfer		
10[a]	FMNH· + N1a = FMN + N1a⁻ + Hi⁺	$V_{10} = k_{10} \cdot$ (FMNH· $\cdot$ N1a – FMN $\cdot$ N1a⁻ $\cdot$ exp(2.3 $\cdot$ (7 – pHi))/K_{eq10})
11[a]	FMNH· + N3 = FMN + N3⁻ + Hi⁺	$V_{11} = k_{11} \cdot$ (FMNH· $\cdot$ N3 – FMN $\cdot$ N3⁻ $\cdot$ exp(2.3 $\cdot$ (7 – pHi))/K_{eq11})
12	N2 + N3⁻ = N2⁻ + N3	$V_{12} = k_{12} \cdot$ (N2 $\cdot$ N3⁻ – N2⁻ $\cdot$ N3/K_{eq12})
13[a]	N2⁻ + CI.Q⁻ + 8 $\cdot$ Hi⁺ = N2 + CI.QH2 + 6 $\cdot$ Ho⁺	$V_{13} = k_{13} \cdot$ (N2⁻ $\cdot$ CI.Q⁻ $\cdot$ exp(2 $\cdot$ 2.3 $\cdot$ (7 – pHi)) – N2 $\cdot$ CI.QH2 $\cdot$ exp(4 $\cdot$ (F$\cdot\Delta\Psi$/R$\cdot T$ + 2.3 $\cdot$ (pHi – pHo)))/K_{eq13})
14	CI.QH2 = CI + QH2	$V_{14} = k_{14} \cdot$ (CI.QH2 – CI $\cdot$ QH2/K_{eq14})
NAD⁺ reduction to NADH in mitochondrial matrix		
15	NAD⁺ = NADH	$V_{15} = k_{15} \cdot$ (NAD⁺ – NADH/K_{eq15})
Superoxide anion (O₂·⁻$_{MX}$) production by Complex I into the mitochondrial matrix		
16	FMNH⁻ + O₂ = FMNH· + O₂·⁻$_{MX}$	$V_{16} = k_{16} \cdot$ (FMNH⁻ $\cdot$ O₂ – FMNH· $\cdot$ O₂·⁻$_{MX}$ /K_{eq16})
17	Q·⁻ + O₂ = Q + O₂·⁻$_{MX}$	$V_{17} = k_{17} \cdot$ (Q·⁻ $\cdot$ O₂ – Q $\cdot$ O₂·⁻$_{MX}$ /K_{eq17})
Superoxide anion dismutation in the mitochondrial matrix		
18	2O₂·⁻$_{MX}$ + 2Hi⁺ → O₂ + H₂O₂ $_{MX}$	$V_{18} = k_{cat18} \cdot E_{tot} \cdot$ O₂·⁻$_{MX}$/(K_{m18} + O₂·⁻$_{MX}$)
Succinate dehydrogenase reaction (Complex II)		
19[b]	Succ + Qn → Fum +QH2n	$V_{19} = V_{max19} \cdot$ Qn/(Qn + QH2n)/(K_{19} + Qn/(Qn + QH2n))
Q and QH2 intramembrane diffusion		
20[c]	QH2n = QH2p	$V_{20} = k_{20} \cdot$ (QH2n – QH2p/K_{eq20})
21[c]	Qp = Qn	$V_{21} = k_{21} \cdot$ (Qp – Qn/K_{eq21})
Q$_o$–site reactions (Complex III)		
22	bL + ISPox + QH2p = bL.QH2.ISPox	$V_{22} = k_{22} \cdot$ (bL $\cdot$ ISPox $\cdot$ QH2p – bL**.**QH2**.**ISPox/K_{eq22})
23[a]	bL**.**QH2.ISPox = bL**.**Q·⁻.ISPH + Ho⁺	$V_{23} = k_{23} \cdot$ (bL**.**QH2.ISPox – bL**.**Q·⁻.ISPH $\cdot$ exp(F $\cdot \delta_1 \cdot \Delta\Psi$/R $\cdot T$ + 2.3 $\cdot$ (7 – pHo)) /K_{eq23})
24	bL**.**Q·⁻.ISPH = bL⁻**.**Q.ISPH	$V_{24} = k_{24} \cdot$ (bL**.**Q·⁻.ISPH – bL⁻**.**Q.ISPH/K_{eq24})
25[a]	bL⁻**.**Q.ISPH + bH = bL**.**Q.ISPH + bH⁻	$V_{25} = k_{25} \cdot$ (bL⁻**.**Q.ISPH $\cdot$ bH– bL**.**Q.ISPH $\cdot$ bH⁻ $\cdot$ exp(F $\cdot \delta_2$ $\cdot \Delta\Psi$/R $\cdot T$)/K_{eq25})
26	bL.Q.ISPH = ISPH + Qp + bL	$V_{26} = k_{25} \cdot$ (bL.Q.ISPH – ISPH $\cdot$ Qp $\cdot$ bL/K_{eq26})
27[a]	ISPH + c1 = ISPox + c1⁻ + Ho⁺	$V_{27} = k_{27} \cdot$ (ISPH $\cdot$ c1 – ISPox $\cdot$ c1⁻ $\cdot$ exp(2.3 $\cdot$ (7 – pHo)) /K_{eq27})
Superoxide anion (O₂·⁻ $_{IMS}$) production by Complex III into the intermembrane space (IMS)		
28	bL**.**Q·⁻.ISPH + O₂ = bL**.**Q.ISPH + O₂·⁻$_{IMS}$	$V_{28} = k_{28} \cdot$ (bL**.**Q·⁻.ISPH $\cdot$ O₂ – bL**.**Q.ISPH $\cdot$ O₂·⁻$_{IMS}$ /K_{eq28})

	Superoxide anion ($O_2^{-}{}_{MX}$) production by Complex III into the mitochondrial matrix	
29	$bL.Q^{·-}.ISPH + O_2 =$ $bL.Q.ISPH + O_2^{·-}{}_{MX}$	$V_{29} = k_{29} \cdot (bL.Q^{·-}.ISPH \cdot O_2 - bL.Q.ISPH \cdot O_2^{·-}{}_{MX} / K_{eq29})$
	Superoxide anion spontaneous dismutation and oxidation by cyt c in IMS	
30	$2O_2^{·-}{}_{IMS} + 2H^+ \rightarrow O_2 + H_2O_2$ IMS	$V_{30} = k_{30} \cdot (O_2^{·-}{}_{IMS})^2$
31	$O_2^{·-}{}_{IMS} + c = O_2 + c^-$	$V_{31} = k_{31} \cdot (O_2^{·-}{}_{IMS} \cdot c - O_2 \cdot c^- / K_{eq31})$
	Q_i–site reactions (Complex III)	
32	$bH^- + Qn = bH^-.Q$	$V_{32} = k_{32} \cdot (bH^- \cdot Qn - bH^-.Q/K_{eq32})$
33[a]	$bH^-.Q + Hi^+ = bH.QH^·$	$V_{33} = k_{33} \cdot (bH^-.Q - bH.QH^· \cdot \exp(F \cdot \delta_3 \cdot \Delta\Psi/R \cdot T - 2.3 \cdot (7 - pHi))/K_{eq33})$
34[a]	$bH.QH^· + bL^-.Q = bH^-.QH^· +$ $bL.Q$	$V_{34} = k_{34} \cdot (bH.QH^· \cdot bL^-.Q - bH^-.QH^· \cdot bL.Q \cdot \exp(F \cdot \delta_2 \cdot \Delta\Psi/R \cdot T)/K_{eq34})$
35[a]	$bH^-.QH^· + Hi^+ = bH.QH2$	$V_{35} = k_{35} \cdot (bH^-.QH^· - bH.QH2 \cdot \exp(F \cdot \delta_3 \cdot \Delta\Psi/R \cdot T - 2.3 \cdot (7 - pHi))/K_{eq35})$
36	$bH.QH2 = bH + QH2n$	$V_{36} = k_{36} \cdot (bH.QH2 - bH \cdot QH2n/K_{eq36})$
	Cytochrome c reduction	
37	$c1^- + c = c1^-.c$	$V_{37} = k_{37} \cdot (c1^- \cdot c - c1^-.c/K_{eq37})$
38	$c1^-.c = c1.c^-$	$V_{38} = k_{38} \cdot (c1^-.c - c1.c^-/K_{eq38})$
39	$c1.c^- = c1 + c^-$	$V_{39} = k_{39} \cdot (c1.c^- - c1 \cdot c^-/K_{eq39})$
	Cytochrome c oxidase reaction (Complex IV)	
40[d]	$2c^- + 4 \cdot Hi^+ + (1/2) \cdot O_2 =$ $2c + H_2O + 2 \cdot Ho^+$	$V_{40} = k_{40} \cdot c^-/c_{tot}/(1 + k_{O2}/O_2) \cdot$ $(\exp(-\Delta G^0/2RT) \cdot \exp(2 \cdot 2.3 \cdot (7 + pHo - 2 \cdot pHi)) \cdot$ $\exp(-\Delta\Psi \cdot F/RT) \cdot O_2^{0.25} \cdot c^- - c \cdot \exp(\Delta\Psi \cdot F/RT))$
	Mitochondrial Glutathione peroxidase (GPx)	
41[e]	$2GSH + H_2O_{2\,MX} \rightarrow$ $GSSG + 2H_2O$	$V_{41} = k_{411} \cdot k_{412} \cdot [E_{tot}] \cdot [H_2O_2] \cdot [GSH]/$ $(k_{411} \cdot [H_2O_2] + k_{412} \cdot [GSH])$
	Mitochondrial Glutathione reductase (GR)	
42[f]	$GSSG + NADPH + H^+ \rightarrow$ $2GSH + NADP^+$	$V_{42} = V_{max42} \cdot [GSSG] \cdot [NADPH] /$ $(K_{m\,NADPH} \cdot [GSSG] + K_{m\,GSSG} \cdot [NADPH] + [GSSG] \cdot$ $[NADPH])$
	H_2O_2 transport through IMM	
43	$H_2O_{2\,MX} = H_2O_{2\,IMS}$	$V_{43} = k_{43} \cdot ([H_2O_{2\,MX}] - [H_2O_{2\,IMS}]/K_{eq43})$
	H_2O_2 transport through OMM	
44	$H_2O_{2\,IMS} = H_2O_{2\,Cyt}$	$V_{44} = k_{44} \cdot ([H_2O_{2\,IMS}] - [H_2O_{2\,Cyt}]/K_{eq44})$
	O_2^{-} transport through OMM	
45	$O_2^{·-}{}_{IMS} = O_2^{·-}{}_{Cyt}$	$V_{45} = k_{45} \cdot ([O_2^{·-}{}_{IMS}] - [O_2^{·-}{}_{Cyt}]/K_{eq45})$

[a]Reactions include steps dependent on membrane potential ($\Delta\Psi$) and/or inside (matrix) and/or outside (intermembrane space) H^+ concentration, pHi and pHo, respectively. The equilibrium constants (K_{eq}) dependence of these reactions on $\Delta\Psi$ were described as $K_{eq}(\Delta\Psi) = K_{eq} \cdot \exp(n \cdot F \cdot \delta \cdot \Delta\Psi/RT)$, where K_{eq} is K_{eq} at $\Delta\Psi = 0$, n is number of electrons or H^+ transferred through a part of the membrane δ. Other constants F, R, and T have usual meaning. The equilibrium constants dependence on pH were described as in the paper [18]: $K_{eq}(pH) = K_{eq} \cdot \exp(2.3 \cdot (7 - pH))$, where K_{eq} is K_{eq} at pH = 7.

[b]Rate equation was taken from experimental observations [19].

[c]Diffusion process was described as in the paper [18].

[d]Rate equation was taken from the theoretical work [20].

[e]Rate equation was derived from the work [21]

[f]Rate equation was derived from the work [22] at the simplest suggestion ping pong mechanism of Glutathione reductase.

Table 2. Parameter values for the model

Reaction No	Midpoint potential $E_m = E$, (mV)	Equilibrium constant K_{eq}	$k_{forward}$	Other parameters	Reference
Electron transfer in Complex I					
1		0.01 μM⁻¹	83 μM⁻¹·s⁻¹		[23][b] [24][c]
2		0.032[d]	1.44·10¹² s⁻¹		[25][c]
3		25 μM	10⁶ s⁻¹		[23][b]
4		0.001 μM⁻¹	0.1 μM⁻¹·s⁻¹		[23][b]
5		0.02 μM⁻¹	2 μM⁻¹·s⁻¹		[23][b]
The first electron transfer					
6	E(FMNH·/ FMNH⁻) = −286 E(N3) = −250	4.2	5·10⁸ μM⁻¹·s⁻¹		[26][a][27][a] [25][c]
7	E(N3) = −250 E(N2) = −100	400	10⁴ μM⁻¹·s⁻¹		[28][a] [24, 29][c]
8		0.1 μM⁻¹	10[f] μM⁻¹·s⁻¹		
9	E(N2) = −100 E(CI.Q/ CI.Q⁻) = −233[f]	0.005[f]	4·10⁵ μM⁻¹·s⁻¹		[28][a][25][c]
The second electron transfer					
10	E(FMN/ FMNH·) = −363 E(N1a) = −370	0.75	2·10⁶ μM⁻¹·s⁻¹	pHi = 7.5	[26][a][27][a] [25][c]
11	E(FMN/ FMNH·) = −363 E(N3) = −250	92	10⁹ μM⁻¹·s⁻¹	pHi = 7.5	[26][a][27][a] [25][c]
12	E(N3) = −250 E(N2) = −100	400	10⁴ μM⁻¹·s⁻¹		[28][a] [24, 29][c]
13		2·10¹³ [f]	2.7·10⁶ μM⁻¹·s⁻¹	pHi = 7.5 pHo = 7.0	[25][c]
14		20[f] μM	1000[f] s⁻¹		
NAD⁺ reduction to NADH in mitochondrial matrix					
15		4.5	0.45 s⁻¹		[20][bc]
Superoxide anion (O₂ₘ⁻) production by Complex I into the mitochondrial matrix					
16	E(O₂/O₂·⁻) = −160 E(FMNH·/ FMNH⁻) = −286	150	2[f] μM⁻¹·s⁻¹		[30][a][26][a]
17	E(Q/Q⁻) = −233[f] E(O₂/O₂·⁻) = −160	18.5[f]	0.04[f] μM⁻¹·s⁻¹		[30][a]
Superoxide anion dismutation catalyzed by MnSOD in the mitochondrial matrix					
18				$k_{cat18} = 4·10^4$ s⁻¹ K_{m18}=50 μM E_{tot}[e] = 3.7 μM	[31] [32]

Succinate dehydrogenase reaction (Complex II)					
19				$K_{19} = 0.6$; $V_{max19} = 256$ mM/min (4270 μM/s)	[19]
Q and QH2 transmembrane diffusion					
20		1	22000 s^{-1}		[18][c]
21		1	22000 s^{-1}		[18][c]
Q_o–site reactions (Complex III)					
22		$10^{-5\,f}$ μM^{-2}	0.1^f μM^{-2}·s^{-1}		
23	$\Delta Em = -200$ mV for the reaction	$3.4 \cdot 10^{-4}$	10^3 s^{-1}	pHo = 7.0 $\delta_1 = 0.2$	[33][abc]
24		55^f μM	10^{5f} s^{-1}		
25		40	10^{5f} μM^{-1}s^{-1}	$\delta_2 = 0.5$	[34][b]
26		$10^{6\,f}$ μM	$5 \cdot 10^{3f}$ s^{-1}		
27	$E_{m(ISPH)} = 300$ $E_{m(c1)} = 270$	0.3	10^{5f} μM^{-1}s^{-1}	pHo = 7.0	[35][abc]
Superoxide anion ($O_2^{\cdot-}$ IMS) production by Complex III into the intermembrane space (IMS)					
28	$E(bL.Q.ISPH/ bL.Q^{\cdot-}.ISPH) = -160$ $E(O_2/O_2^{\cdot-}) = -160$	1	2 μM^{-1}·s^{-1}		[18][a] [30][a]
Superoxide anion ($O_2^{\cdot-}$ MX) production by Complex III into the mitochondrial matrix					
29	$E(bL.Q.ISPH/ bL.Q^{\cdot-}.ISPH) = -160$ $E(O_2/O_2^{\cdot-}) = -160$	1	2 μM^{-1}·s^{-1}		[18][a] [30][a]
Superoxide anion spontaneous dismutation and oxidation by cyt c in the intermembrane space (IMS)					
30			0.6 μM^{-1}·s^{-1}	pHo = 7.0	[36][c]
31	$E(O_2/O_2^{\cdot-}) = -160$ $E_{m(c)} = 263$	$2.2 \cdot 10^7$	0.26 μM^{-1}·s^{-1}		[30][a] [37][a] [38, 39][c]
Q_i–site reactions (Complex III)					
32		0.022 μM^{-1}	1 μM^{-1}·s^{-1}		[40][b]
33		55	$5 \cdot 10^4$ s^{-1}	pHi = 7.5 $\delta_3 = 0.3$	
34		40	$10^{5\,f}$ s^{-1}	$\delta_2 = 0.5$	[34][b]
35		0.67	$10^{5\,f}$ s^{-1}	pHi = 7.5 $\delta_3 = 0.3$	
36		45 μM	500^f s^{-1}		[40][b]
Cytochrome c reduction					
37		1.17	$2 \cdot 10^3$ μM^{-1}·s^{-1}		[41, 42][bc]
38	$E_{m(c1)} = 270$ $E_{m(c)} = 263$	0.8	$1.4 \cdot 10^4$ s^{-1}		[35][a] [37][a] [41, 42][c]
39		0.85	$1.7 \cdot 10^3$ s^{-1}		[41, 42][bc]
Cytochrome c oxidase reaction (Complex IV)					
40			100^f s^{-1}	$k_{O2} = 1$ μM; $\Delta G^0 = -122.94$ kJ·mol^{-1}; pHi = 7.5 pHo = 7.0	[20]

Glutathione peroxidase					
41				$k_{411} = 41\ \mu M^{-1} \cdot s^{-1}$ $k_{412} = 0.23\ \mu M^{-1} \cdot s^{-1}$ $[E_{tot}]^g = 1.77\ \mu M$	[43]
Glutathione reductase					
42				$V_{max42}{}^h = 196.44\ \mu M/s$ $K_{m\ NADPH} = 63\ \mu M;$ $K_{m\ GSSG} = 154\ \mu M;$ $[NADPH]^i = 85\ \mu M$	[44], [45]
H₂O₂ transport through IMM					
43		1	$30^j\ s^{-1}$		
H₂O₂ transport through OMM					
44		1	$30^j\ s^{-1}$	$[H_2O_{2\ Cyt}] = 1 \cdot 10^{-8}\ M$	[46]
O₂·⁻ transport through OMM					
45		1	$500^k\ s^{-1}$	$[O_2 \cdot^-{}_{Cyt}] = 2.5 \cdot 10^{-11}\ M$	[9]^c, [46]

[a]Reference for the midpoint redox potential E_m

[b]Reference for the equilibrium constant K_{eq}

[c]Reference for the forward rate constant $k_{forward}$

[d]Value used is computed from the relation $K_{eq1} \cdot K_{eq2} \cdot K_{eq3} = \exp(2 \cdot F \cdot (E_{FMN} - E_{NAD+})/R \cdot T)$ in accord with the thermodynamic cycle pointed out by Kussmaul and Hirst [26], where midpoint redox potentials $E_{FMN} = -380$ mV (pH 7.0) and $E_{NAD+} = -320$ mV (pH 7.0), respectively, [27] and F, R and T have usual meaning.

[e]Value used was calculated from experimental data on Mn-SOD content in liver mitochondria which is around of 8.8 nmol/g prot [32]. Taking into account that 1 nmol/mg protein = 275 μM and matrix water space fraction $W_{MX} = 0.6514$, concentration of Mn-SOD normalized by mitochondrial matrix volume equals to 0.0088·275 μM /0.6514 = 3.7 μM (see **Section 5** for detail).

[f]Values adjusted to match experimental data on kinetics of superoxide production.

[g]$[E_{tot}]$ value was calculated from the equation $V_{41} = k_{411} \cdot k_{412} \cdot [E_{tot}] \cdot [H_2O_2] \cdot [GSH]/$ $(k_{411} \cdot [H_2O_2] + k_{412} \cdot [GSH])$ for the rate of GPx reaction (Table 1) at the following values of kinetic parameters. As shown above in Table 2, $k_{411} = 41\ \mu M^{-1} \cdot s^{-1}$ and $k_{412} = 0.23\ \mu M^{-1} \cdot s^{-1}$. Besides, experimentally observed activity of mitochondrial GPx–1 which accord with the rate V_{41} is of 219 nmol/min/mg protein at [H₂O₂]=200 μM and [GSH] ≈ 10 nmol/mg protein ([GSH] equals approximately the total mitochondrial glutathione content at the experimental measure of GPx activity) [11]. Taking into account that 1 nmol/mg protein = 275 μM and matrix water space fraction $W_{MX} = 0.6514$, concentration [GSH] and the rate V_{41} normalized by mitochondrial matrix volume equals to 10 · 275 μM /0.6514 = 4222 μM and 219 · 275 μM /0.6514/60 s = 1540 μM/s, respectively. It results in the value of matrix GPx–1 concentration $[E_{tot}] = 1.77$ μM.

[h]V_{max42} was calculated from the equation $V_{42} = V_{max42} \cdot [GSSG] \cdot [NADPH]/$ $(K_{m\ NADPH} \cdot [GSSG] + K_{m\ GSSG} \cdot [NADPH] + [GSSG] \cdot [NADPH])$ for the rate of GR reaction (Table 1) at $K_{m\ NADPH} = 63$ μM and $K_{m\ GSSG} = 154$ μM [44] as shown above in Table 2. Besides, experimentally observed mitochondrial GR activity, V_{42}, equals to 22 nmol/min/mg prot. at [NADPH] = 0.255 mM and [GSSG] = 7 mM [47]. Taking into account that the rate V_{42} normalized by mitochondrial matrix volume equals to 22 · 275 μM/0.6514/60 s = 154.8 μM/s we get $V_{max42} = 196.44$ μM/s.

[i]Value used is derived from experimental data [45] at the following suggestions. Experimentally observed values of mitochondrial NADPH level vary from 0.15 to 0.25 nmol/mg mit protein [45], so, we took medium value of NADPH equal to 0.2 nmol/mg mit protein which corresponds matrix concentration [NADPH] = 0.2·275 μM /0.6514 ≈ 85 μM

[j]Value used equals to the rate constant of the water flux through IMM and OMM [48].

[k]Value used is a computer modeling result.

Conserved moeties (nmol/mg mitochondrial protein): Complex I content which changes in different tissues from 0.1 to 0.4 [49, 50] was taken of 0.2, values of total ubiquinone and Complex III content were taken as follows [12], [total Q] = 4, [total cyt bL] = [total cyt bH] =

70

[total cyt c1] = [total ISP] = 0.325. Translation of whole membrane concentration expressed in nmol/mg mit.prot. to local protein concentration expressed in µM presented in **Section 2.5.** Besides, [total cyt c] = 700 µM [51] and [total mitochondrial Glutathione] = 10 nmol/mg protein [11] which according to matrix concentration 4222 µM.

2. Detailed kinetic model of Complex I

Initial steps of electron transfer in Complex I (reactions 1–5) were taken from the kinetic model developed by Kussmaul and Hirst [26] for isolated Complex I. In this model Kussmaul and Hirst proposed that superoxide is formed by the transfer of one electron from the fully reduced flavin $FMNH^-$ to O_2 (reaction 16 in Fig. 1 and Table 1). Detailed analysis of $NADH/NAD^+$ binding to Complex I is reviewed by Vinogradov [52]. In the kinetic description of electron transfer through the chain of Fe-S clusters we took into account the generally accepted suggestion that $FMNH^-$ donates the first electron to the Fe-S cluster N3 (reaction 6). Electron transfer from N3 to the terminal cluster N2 through the chain of equipotential redox centers N1b, N4, N5, N6a, and N6b [27] is approximated as a single step (reaction 7) with an apparent rate constant of 10^4 s^{-1} since electron movement through the entire chain takes about 100 µs [24, 29]. Subsequently, the first electron transfers from N2 to ubiquinone (Q) bound to Complex I (reactions 8, 9), reducing ubiquinone to semiquinone.

The second electron transfers from the semireduced flavin radical $FMNH^.$ to either cluster N1a or cluster N3 (reactions 10 and 11). Electron transfer from cluster N1a to cluster N3 is very slow ($k_{forward}$ is about of 160 s^{-1} [25]) compared to other reactions in Complex I, so we propose that cluster N1a only deposits single electrons without their delivery to the chain of seven redox centers. A kinetic model of electron transfer in the membrane domain of Complex I and the coupling mechanism of proton translocation through the membrane takes into account recent X-ray structures of complex I and the hypothesis of a "piston" mechanism of transmembrane H^+ movement, as reported by Sazanov and colleagues [53]. It is very likely, in accord with this mechanism that 3 H^+ move through the mitochondrial membrane simultaneously during electron transfer from N2 to quinone. We propose that a conformational switch and translocation of 3 H^+ occurs during electron transfer from reduced $N2^-$ to ubisemiquinone to form QH_2 (reaction 13) reflecting the experimentally observed increase in ubisemiquinone concentration upon an increase in $\Delta\mu_{H+}$ [54, 55].

The path of the fourth proton translocation in Complex I is not clear [53]. It is very likely that the fourth proton transfer is also controlled by a conformational switch in the membrane arm [56]. We propose that the fourth H^+ translocation is also coupled with electron transfer from reduced $N2^-$ to semiquinone (reaction 13). Therefore, we suggest that 4 H^+ move through the mitochondrial membrane simultaneously in reaction (13).

Reactions 8 and 14 in Fig. 1 and Table 1 describe binding and dissociation of Qn and QH2n, respectively, in the quinone-binding site where the subscript "n" refers to the negative side of the inner membrane.

Furthermore, we hypothesize that semiquinone $Q^{.-}$ in the complex $CI.Q^{.-}$ (Fig. 1 and Table 1) is the second site of superoxide formation in Complex I (reaction 17). This hypothesis is supported by numerous experimental evidence that ubisemiquinone can be one of the sites of superoxide generation in Complex I (for review see [57]).

3. Detailed kinetic model of Complex III

Fully reduced quinone QH2n generated by Complex I or Complex II (reaction 19) transports to the positive side of the inner membrane (reaction 19), and QH2p is doubly oxidized at the Qo-site of Complex III (reactions 22–26). Then, oxidized Qp is transported from the positive to the negative side of the inner membrane (reaction 20), and Qn is doubly reduced at the Qi-site of Complex III (reactions 32–36) completing Mitchell's Q-cycle [58] after binding and oxidation of the second QH2p molecule at the Qo-site.

The kinetic scheme of QH2p oxidation at the Qo-site is based mainly on the work of Crofts and colleagues [59]. They suggested the initial formation of an ES-complex (the complex bL.QH2.ISPox in Fig. 1) at the Qo-site (reaction 22) with the following bifurcated reaction where the first electron of QH_2 is transferred to the high-potential chain, consisting of ISP (reaction 23) and cyt c1 (reaction 27). The second electron is transferred from the semiquinone $Q^{\cdot-}$ to the low-potential chain, consisting of cyt bL (reaction 24) and cyt bH (reaction 25). Crofts and colleagues [59] proposed, that reduced iron-sulfur protein ISPH (extrinsic domain of ISP) moves from the b-position to the c1-position (reaction 24) before the second electron passes to cyt bL. However, another hypothesis [60] suggests that the conformational switch of ISPH occurs only after the second electron transfers from cyt bL to bH. We propose the second hypothesis [60] in the current work. Based on direct experimental observations [61] it is generally accepted that the semiquinone $Q^{\cdot-}$ of the Qo-site (complex bL.$Q^{\cdot-}$) is the site of superoxide formation in Complex III. This superoxide is released to the IMS and matrix (reactions 28, 29) [4].

All other reactions are described in detail in Tables 1 and 2.

4. Computational model

A computational model consisting of 35 ordinary differential equations (ODE) and 14 moiety conservation equations was derived from the reaction network using the law of mass action, Michaelis and Hill kinetics for all 45 kinetic processes. All equations are presented below. The model was implemented in DBSolve Optimum software available at website **http://insysbio.ru** . The details of the mathematical model describe oxidized and reduced states of different carriers and electron flows through Complexes I, II, III and IV. Values of model parameters, rate constants and concentration of different electron carriers, were taken from literature experimental data on thermodynamics and kinetics of electron transfer in respiratory chain (Tables 1 and 2).

5. Dimension of local and whole mitochondrial concentration and rates

Experimental data on intramembrane protein concentration presented in Table 2 in nmole/mg mit. prot. while we use μM for concentration in our computational model. Moreover, we use in the model local concentration of proteins in different fractions of mitochondrion which normalized by volume of these fractions. So, NADH and matrix superoxide concentration normalized by the matrix volume (V_{MX}), cyt c and superoxide in the intermembrane space (IMS) normalized by the IMS volume (V_{IMS}), and concentration of all intramembrane proteins of respiratory chain normalized by the volume of the inner membrane (V_{IMB}). First, we normalized concentration of all proteins by total mitochondrial volume V_{MIT} and then whole mitochondrial concentration translated to local concentration using space fractional ratio of matrix ($W_{MX} = V_{MX}/V_{MIT}$), IMS ($W_{IMS} = V_{IMS}/V_{MIT}$) and the inner membrane ($W_{IMB} = V_{IMB}/V_{MIT}$) of the total mitochondrial volume. In order to calculate matrix water space fraction W_{MX} and IMS water fraction W_{IMS} we used the following experimental data. Mitochondrial water weight fraction and mitochondrial density is of 0.664 g/g and 1.09 g/ml, respectively [62]. That means that mitochondrial water space fraction, W_{MIT}, is of 0.664·1.09 = 0.724. Taking into account that $W_{IMS} \approx 1/14 \approx 0.072$ for the orthodox mitochondria configuration [51], matrix water space fraction $W_{MX} = W_{MIT} - W_{IMS} = 0.724 - 0.072 = 0.652$. It should notice that values of W_{IMS} and W_{MX} coincide with those used in [63].Value of W_{IMB} was calculated as follows. Volume and inner membrane area of the average mitochondrion are of 0.27 μm^3 and 6.47 μm^2, respectively [64]. Suggesting the overage thickness of inner membrane about 0.01 μm we get the inner membrane space fraction (W_{imb}) in mitochondrion of about 0.24. Mitochondrial protein weight fraction W_{wprot} is about 0.25 g/g [62]. Therefore, 1 mg mit. prot. corresponds to 4 mg whole mitochondria and

takes 4 mg/1090 mg/ml = $3.67 \cdot 10^{-3}$ ml = $3.67 \cdot 10^{-6}$ l. So, common used content 1 nmol/ mg mitochondrial protein is equal to whole mitochondrial concentration 10^{-9} mole/ $3.67 \cdot 10^{-6}$ l = 1 mM/3.67 $\approx$ 273 μM which normalized by whole mitochondrial volume, i.e. 1 μM = 3.67 pmol/mg mit prot. In order to get local concentration of different proteins in the matrix, IMS and inner membrane whole mitochondrial concentration were divided by W_{MX}, W_{IMS} and W_{IMB}, respectively. Then, total local intramembrane concentration of ubiquinone Q and Complexes I and III had the following values: total Q = 4 nmol/ mg mit prot = $4 \cdot 10^{-9}$ mole /$3.67 \cdot 10^{-6}$ l /0.24 = 4541 μM; ISP = bL = bH = cyt c1 = 0.325 nmol/ mg mit prot = $0.325 \cdot 10^{-9}$ mole /$3.67 \cdot 10^{-6}$ l /0.24 = 369 μM; FMN = N3 = N1a = N2 = 0.2 nmol/ mg mit prot = $0.2 \cdot 10^{-9}$ mole /$3.67 \cdot 10^{-6}$ l /0.24 = 227 μM. In order to present computer simulated rates of respiration and ROS production which occur only in the inner membrane as the whole mitochondrial rates we multiplied all the rates of intramembrane processes by W_{IBM} = 0.24. In addition, in order to compare computer simulated rates of respiration and ROS production presented in the current paper in μM/s with experimentally observed rates expressed in pmol/min/mg mit. prot. the computer simulated rates should be multiplied by factor $3.67 \cdot 60 = 220$, i.e. 1 μM/s = 220 pmol/min mg mit prot.

RESULTS AND DISCUSSION

1. Analysis of the effect of chronic ethanol-induced inhibition of Complexes I, III and IV on the rate of ROS generation in the mitochondrial respiratory chain

In order to simulate computationally the effects of chronic ethanol exposure on ROS production in mitochondria we took into account experimentally observed chronic ethanol-induced alterations in different segments of the respiratory chain [13–15] and glutathione peroxidase and reductase reactions [11, 16]. First, we analyzed the effects of alterations in the respiratory chain which include a decrease in the content of FeS redox centers in Complex I and cyt b in Complex III, and the catalytic activity of cytochrome c oxidase [13–15]. The effects of the simultaneous 2- and 4-fold decrease in the level of FeS redox center and cyt b, and the catalytic rate constant of cytochrome c oxidase, k_{40} (Table 1), on the rate of superoxide generation by different sites of the respiratory chain during oxidation of NADH alone, succinate alone, and NADH + succinate are shown in Fig. 2, Fig. 3, and Fig. 4, respectively. The control condition corresponds to the following kinetic parameter values presented in Table 2: the content of FeS = 0.2 and cyt b = 0.325 nmol/ mg mit prot; k_{40} = 100 s^{-1} (solid black curves in Fig. 2–4). In accord with these parameter values, the 2-fold decrease corresponds to FeS = 0.1 and cyt b = 0.1625 nmol/ mg mit prot; k_{40} = 50 s^{-1} (red dashed curves) and the 4-fold decrease corresponds to FeS = 0.05 and cyt b = 0.0813 nmol/ mg mit prot; k_{40} = 25 s^{-1} (blue dash-dot curves).

Fig. 2,A–D present a computer simulated steady-state ΔΨ dependency of the superoxide production rate total (Fig. 2,A) and by different sites of Complex I (Fig. 2,B and 2,C) and Complex III (Fig. 2,D) during oxidation of NADH alone. Results presented in Fig. 2,A show a considerable increase in the total rate of superoxide production during inhibition of the respiratory chain over the range of membrane potential of approximately 50 < ΔΨ < 170 mV. This increase occurs due to a strong increase in the rate of superoxide generation at the site FMNH$^-$ of Complex I under the same condition (Fig. 2,B). The superoxide production rate by the second site of Complex I, the semiquinone CI.Q$^{.-}$, is little affected by chronic ethanol-induced depression of the respiratory chain (Fig. 2,C). The effect of chronic ethanol-induced inhibition of Complexes I, III and IV on the rate of superoxide generation by the unstable semiquinone of Complex III, the complex bL.Q$^{.-}$.ISPH in Fig. 1, is more complex and depends on the membrane potential (Fig. 2,D). As Fig. 2,D shows the rate of superoxide generation in Complex III decreases at ΔΨ > 120 mV, increases at ΔΨ < 90 mV and has non-monotonic changes at 90 < ΔΨ < 120 mV upon depression of the respiratory chain. These

chronic ethanol and $\Delta\Psi$ dependent changes in the rate of superoxide generation by different sites of the respiratory chain are related directly to the chronic ethanol and $\Delta\Psi$ dependency of the respiration rate during oxidation of NADH alone (Fig. 2,E).
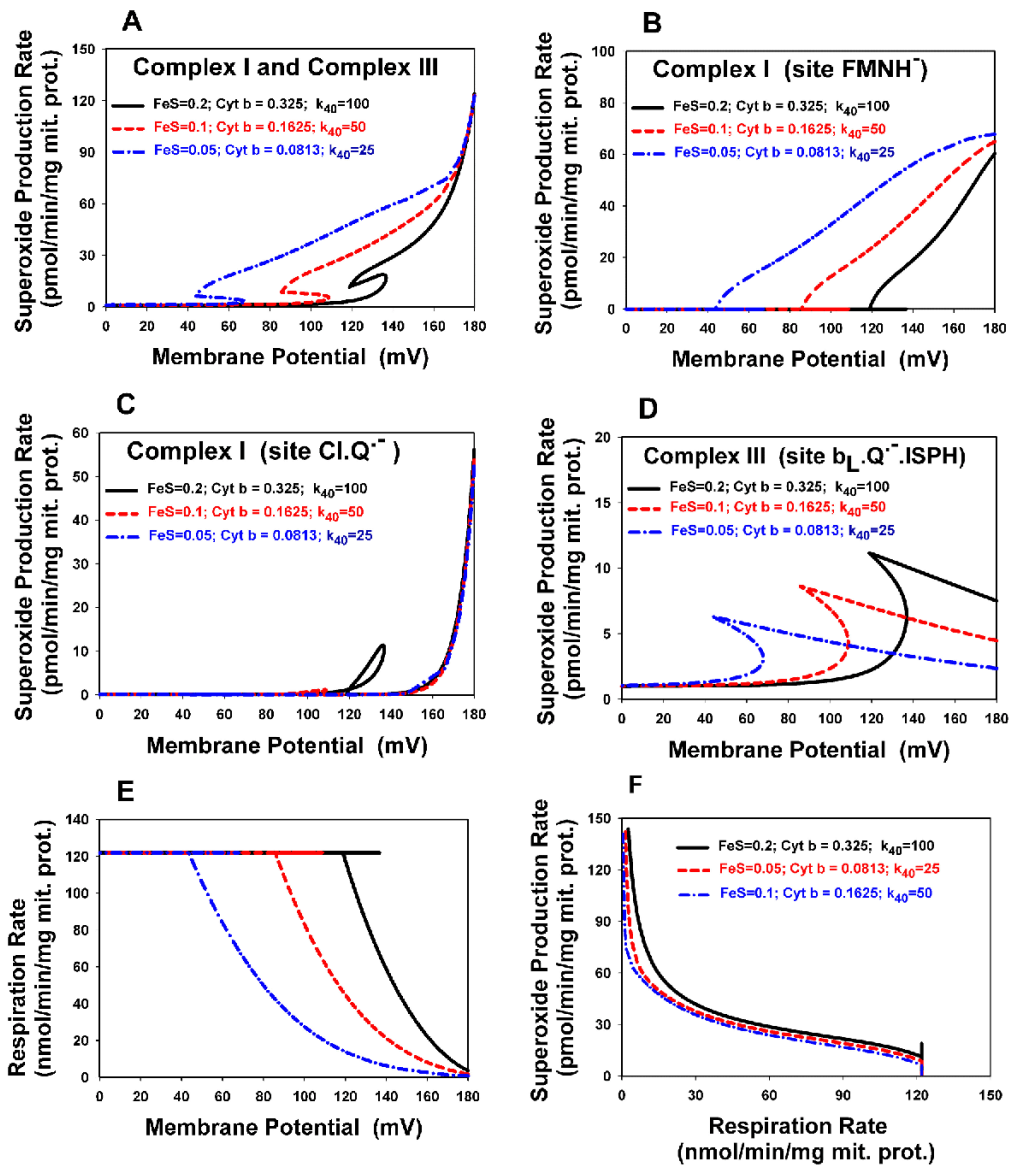

Figure 2. Computer simulated changes in the steady-state rates of respiration and superoxide production upon chronic ethanol-induced alterations in different segments of the respiratory chain during oxidation of NADH alone. Computer simulation was carried out with the mathematical model at kinetic parameter values presented in Table 2. Different curves (black solid, red dashed and blue dash-dot curves) correspond to different values of the levels of FeS redox centers in Complex I and cytochrome b in Complex III, and the catalytic rate constant, k_{40}, of cytochrome c oxidase. Black solid curves correspond to the control values – FeS = 0.2 nmol/ mg mit prot; cyt b = 0.325 nmol/ mg mit prot; k_{40} = 100 s^{-1}. Red dashed curves – FeS = 0.1 nmol/ mg mit prot; cyt b = 0.1625 nmol/ mg mit prot; k_{40} = 50 s^{-1}. Blue dash-dot curves – FeS = 0.05 nmol/ mg mit prot; cyt b = 0.0813 nmol/ mg mit prot; k_{40} = 25 s^{-1}. Designation for every curve is also shown in Fig. 2. **(A)** The total rate of superoxide production by Complexes I and III. **(B–D)** The rate of superoxide generation by different sites of Complexes I and III: **(B)** the site FMNH$^-$ of Complex I; **(C)** the semiquinone of Complex I (site CI.Q$^{\cdot-}$); **(D)** the unstable semiquinone of Complex III (site bL.Q$^{\cdot-}$.ISPH). **(E)** The steady-state respiration rate at different values of the membrane potential. **(F)** Relationships between rates of superoxide production and respiration. All these computer simulated results were obtained during oxidation of NADH alone, i.e. k_{15} = 0.3 s^{-1} and V_{max19} = 0.

First, we consider a $\Delta\Psi$ dependency of the rate of superoxide generation by different sites of the respiratory chain under control condition which presented with black solid curves in

Fig. 2. The steady-state rate of respiration in the control (black solid curve in Fig. 2,E) increases with a decrease in the membrane potential and becomes saturated at $\Delta\Psi \approx 120$ mV due to the almost complete oxidation of NADH and QH2. Saturation of the respiration rate results in a drastic decrease in the rate of superoxide generation by the FMNH$^-$ site of Complex I (Fig. 2,B) and the unstable semiquinone of Complex III (Fig. 2,D) at $\Delta\Psi < 120$ mV. A monotonic decrease in the rate of superoxide generation by the FMNH$^-$ site of Complex I with decreasing $\Delta\Psi$ from 180 to 120 mV (Fig. 2,B) is accounted for by monotonic decreasing NADH and FMNH$^-$, respectively, during monotonic increasing the rate of respiration. By contrast, the rate of superoxide generation by the unstable semiquinone of the Qo-site of Complex III, the complex bL.Q$^{\cdot-}$.ISPH in Fig. 1, increases with decreasing $\Delta\Psi$ from 180 to 120 mV (Fig. 2,D) due to the increasing concentration of the upstream complex bL.QH2.ISP$_{ox}$ (Fig. 1). The concentration of the complexes bL.QH2.ISP$_{ox}$ and bL.Q$^{\cdot-}$.ISPH increases at $120 < \Delta\Psi < 180$ mV for the following reason. Increasing the rate of respiration with decreasing $\Delta\Psi$ from 180 to 120 mV under control condition (black solid curve in Fig. 2,E) results in opposite changes in the concentration of electron carriers bL, ISP$_{ox}$ and QH2 which form the complex bL.QH2.ISP$_{ox}$ (see Fig. 1). The concentration of oxidized cyt bL and ISP$_{ox}$ increases while the concentration of QH2 decreases with increasing respiration rates (data are not shown). The simultaneous increase in the oxidized form of cyt b_L and ISP$_{ox}$ is steeper compared to a decrease in the concentration of QH2 with the increasing rate of respiration. Therefore, this results in an increase in the concentration of the complexes bL.QH2.ISP$_{ox}$ and bL.Q$^{\cdot-}$.ISPH as well as in the rate of superoxide generation by Complex III with a decrease in $\Delta\Psi$ from 180 to 120 mV. Saturation of the respiration rate at $\Delta\Psi \approx 120$ mV is accompanied by a considerable decrease in the concentration of QH2 and complexes bL.QH2.ISP$_{ox}$ and bL.Q$^{\cdot-}$.ISPH (data are not shown) which result in a drastic decrease in the rate of superoxide generation by Complex III as shown by the black solid curve in Fig. 2,D. Results presented in Fig. 2,C show a very high $\Delta\Psi$ sensitivity of the rate of superoxide generation by the semiquinone of Complex I, the site CI.Q$^{\cdot-}$ in Fig. 1. This is accounted for by a high $\Delta\Psi$ sensitivity of the reduction of the semiquinone CI.Q$^{\cdot-}$ to CI.QH$_2$ (reaction 13 in Fig. 1 and Table 1) which is coupled with electrogenic transport of 4 H$^+$ through the inner mitochondrial membrane. A peak in a $\Delta\Psi$ dependency of the rate of superoxide generation by the site CI.Q$^{\cdot-}$ at $\Delta\Psi$ around of 130 mV under control condition (black solid curve in Fig. 2,C) is accounted for by a peak in the concentration of the semiquinone CI.Q$^{\cdot-}$ which results from a drastic increase in the concentration of oxidized ubiquinone (free, Q, and bound to Complex I, CI.Q) at this values of the membrane potential. An additional reason for this peak is a slow decrease in the steady-state concentration of the reduced redox center N2$^-$, electron donor for Q, with decreasing $\Delta\Psi$ from 180 to approximately 120 mV (data are not shown). As to hysteresis in a $\Delta\Psi$ dependency of different rates of ROS production presented in Fig. 2,A–D, this is an intrinsic feature of the respiratory chain which was analyzed in detail elsewhere [65].

The effect of chronic ethanol-induced inhibition of the respiratory chain on the $\Delta\Psi$ dependency of the respiration rate is presented in Fig. 2,E. The computer simulated 2- and 4-fold decrease in the content of FeS redox centers in Complex I and cyt b in Complex III, and the catalytic rate constant of cytochrome c oxidase, k_{40}, results in a considerably slower increase in the steady-state rate of respiration with a decrease in the membrane potential compared to the control (Fig. 2,E) which is very compatible with our laboratory experimental observations of ethanol-induced inhibition of the respiratory rate during oxidation of glutamate plus malate in liver mitochondria isolated from control and ethanol feeding rats (Fig. 1,C in [12]). As a result, the computer simulated steady-state rate of superoxide generation total (Fig. 2,A) and by the site FMNH$^-$ (Fig. 2,B) also decreases at a slower rate with decreasing the membrane potential and becomes negligible at $\Delta\Psi \approx 90$ mV and $\Delta\Psi \approx 50$ mV which corresponds to values of the membrane potential of saturation of the respiration rate under 2- and 4-fold inhibition of the respiratory chain. An initial increase in the rate of

75

superoxide generation by the unstable semiquinone of Complex III with decreasing the membrane potential from 180 mV is followed by a drastic decrease in superoxide production at $\Delta\Psi \approx 90$ mV and $\Delta\Psi \approx 50$ mV under 2- and 4-fold inhibition of the respiratory chain for the reason pointed above.
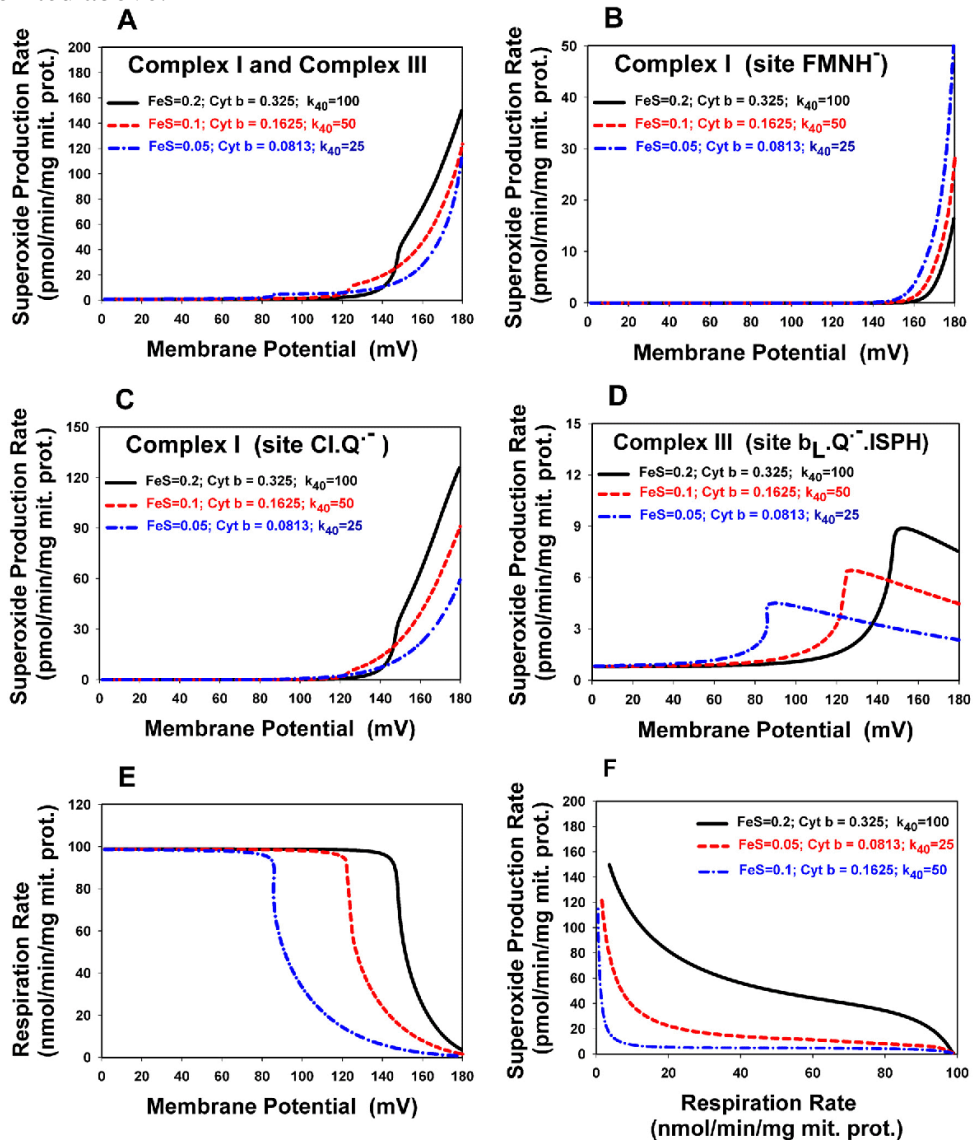

Figure 3. Computer simulated changes in the steady-state rates of respiration and superoxide production upon chronic ethanol-induced alterations in different segments of the respiratory chain during oxidation of succinate alone. Computer simulation was carried out with the mathematical model at kinetic parameter values presented in Table 2. Different curves (black solid, red dashed and blue dash-dot curves) correspond to different values of the levels of FeS redox centers in Complex I and cytochrome b in Complex III, and the catalytic rate constant, k_{40}, of cytochrome c oxidase. Black solid curves correspond to the control values – FeS = 0.2 nmol/ mg mit prot; cyt b = 0.325 nmol/ mg mit prot; $k_{40} = 100$ s^{-1}. Red dashed curves – FeS = 0.1 nmol/ mg mit prot; cyt b = 0.1625 nmol/ mg mit prot; $k_{40} = 50$ s^{-1}. Blue dash-dot curves – FeS = 0.05 nmol/ mg mit prot; cyt b = 0.0813 nmol/ mg mit prot; $k_{40} = 25$ s^{-1}. Designation for every curve is also shown in Fig. 3. (**A**) The total rate of superoxide production by Complexes I and III**. (B–D**) The rate of superoxide generation by different sites of Complexes I and III: (**B**) the site FMNH$^-$ of Complex I; (**C**) the semiquinone of Complex I (site CI.Q$^{\cdot-}$); (**D**) the unstable semiquinone of Complex III (site bL.Q$^{\cdot-}$.ISPH). (**E**) The steady-state respiration rate at different values of the membrane potential. (**F**) Relationships between rates of superoxide production and respiration. All these computer simulated results were obtained during oxidation of succinate alone, i.e. $k_{15} = 0$ and $V_{max19} = 3000$ μM/s.

The computer simulated relationship between the rates of total superoxide generation in the mitochondrial respiratory chain and respiration during oxidation of NADH alone (Fig. 2,F) shows an unexpected decrease in the ratio of rates of superoxide production and

respiration upon chronic ethanol-induced inhibition of the respiratory chain. The most considerable decrease in this ratio is observed at a high value of the membrane potential with a low rate of respiration. These results require some explanation. The all curves in Fig. 2,F were drawn from $\Delta\Psi$ dependencies of rates of superoxide production and respiration presented in Fig. 2,A and Fig. 2,E, i.e. obtained at different values of the membrane potential which is fixed parameter in our computational model. This means that the same value of the rate of respiration for different curves was obtained at different values of the membrane potential. Therefore, a decrease in the rate of superoxide production at the same the respiratory rate upon inhibition of the respiratory chain relates to a decrease in the membrane potential. More detailed explanation of relationships between the rates of total superoxide generation in the mitochondrial respiratory chain and respiration upon inhibition of the respiratory chain will be done below at consideration of oxidation of succinate alone (Fig. 3,F).

Fig. 3 presents the computer simulated effect of chronic ethanol-induced inhibition of the respiratory chain on the steady-state rates of respiration and superoxide production during oxidation of succinate alone at different values of the membrane potential. Chronic ethanol-induced inhibition of the respiratory chain is simulated by the simultaneous 2- and 4-fold decrease in the level of FeS redox center and cyt b, and the catalytic rate constant of cytochrome c oxidase, k_{40}, just as in the previous case of oxidation of NADH alone presented in Fig. 2.

In contrast to oxidation of NADH alone, chronic ethanol-induced changes in the total rate of superoxide production by the respiratory chain during oxidation of succinate alone are non-monotonic and depend on the membrane potential (Fig. 3,A). The total rate of superoxide production increases over the entire range of membrane potential below a $\Delta\Psi$ of approximately 145 mV and it decreases at $\Delta\Psi > 145$ mV upon inhibition of Complexes I, III and IV. Such non-monotonic changes in the total rate of superoxide production result from non-monotonic changes in the rate of superoxide generation by the semiquinone of Complex I (Fig. 3,C) as the main site of superoxide generation in the respiratory chain during oxidation of succinate alone. A considerable decrease in the rate of superoxide generation by the semiquinone of Complex I at high values of the membrane potential upon chronic ethanol-induced inhibition of the respiratory chain are accounted for by a decrease in the respiration rate under this condition and, as a consequence, a considerable decrease in the concentration of oxidized Q which participates in formation of the superoxide generating site CI.Q$^-$ (Fig. 1). The rate of superoxide generation by the site FMNH$^-$ increases upon chronic ethanol-induced inhibition of the respiratory chain (Fig. 3,B) due to inhibition of the rate of respiration and more reduced state of flavine.

Chronic ethanol-induced changes in the rate of superoxide generation by the unstable semiquinone of Complex III during oxidation of succinate alone (Fig. 3,D) resemble those during oxidation of NADH alone (Fig. 2,D) and also depend on the membrane potential. An initial increase in the rate of superoxide generation by the unstable semiquinone of Complex III with decreasing the membrane potential from 180 mV is followed by a drastic decrease in superoxide production at $\Delta\Psi \approx 145$ mV, $\Delta\Psi \approx 125$ mV and $\Delta\Psi \approx 85$ mV under the control condition, 2- and 4-fold inhibition of the respiratory chain, respectively. These values of the membrane potential just correspond to a $\Delta\Psi$ of saturation of the respiration rate during oxidation of succinate alone (Fig. 3,E). A relationship between rates of total superoxide production and respiration during oxidation of succinate alone (Fig. 3,F) shows a very high decrease in the ratio of rates of superoxide production and respiration upon chronic ethanol-induced inhibition of the respiratory chain. This is accounted for by the following two factors. First, curves of a computer simulated steady-state $\Delta\Psi$ dependency of the respiration rate shift considerably to low values of the membrane potential upon chronic ethanol-induced inhibition of the respiratory chain (Fig. 3,E) and, second, the total rates of superoxide production decline steep with decreasing the membrane potential and become negligible at $\Delta\Psi < 120$ mV under

77

the same condition (Fig. 3,A). This results in a considerable decrease in the total rate of superoxide production at any fixed value of the respiration rate upon chronic ethanol-induced inhibition of the respiratory chain. Consider, for instance, the value of the respiration rate of 20 nmol/min/mg mit. prot. in Fig. 3,E and 3,F. As Fig. 3,E shows the respiration rate takes the value of 20 nmol/min/mg mit. prot. at $\Delta\Psi \approx 165$ mV, $\Delta\Psi \approx 145$ mV and $\Delta\Psi \approx 110$ mV under the control condition, 2- and 4-fold inhibition of the respiratory chain, respectively. The total rates of superoxide production corresponding to these values of $\Delta\Psi$ (165, 145 and 110 mV) decrease considerably upon chronic ethanol-induced inhibition of the respiratory chain (Fig. 3,A) just as presented in Fig. 3,F. In order to avoid any confusion at interpretation of relationships between rates of total superoxide production and respiration presented in Fig. 3,F we would like to point out that a considerable decrease in the rate of superoxide production at the same respiratory rate upon 2- and 4-fold inhibition of the respiration chain is accounted for by a decrease in the membrane potential only which is a fixed parameter in our computational model. Therefore, each of the curves presented in Fig. 3,F should be considered separately as a sample of that how relationship between rates of total superoxide production and respiration changes upon chronic ethanol-induced inhibition of the respiratory chain during oxidation of succinate alone.

It should be pointed out that inhibition of the respiratory rate over the range of membrane potential below a $\Delta\Psi$ of approximately 180 mV obtained above computationally is compatible with experimental observations of ethanol-induced inhibition of the respiratory rate during oxidation of succinate alone in liver mitochondria isolated from control and ethanol feeding rats (Fig. 1,B in [12]).

Computer simulated results of the effect of inhibition of the respiratory chain on the steady-state rates of respiration and superoxide production during oxidation of NADH + succinate at different values of the membrane potential are presented in Fig. 4. These results predict that a $\Delta\Psi$ dependency of all steady-state characteristics are very similar to those observed during oxidation of NADH alone presented in Fig. 2. However, there is a difference between them which relates to the rate of respiration for the following reason. When the respiratory chain is fueled by two substrates, NADH and succinate, through different inputs, a competition arises between Complexes I and II for oxidized ubiquinone Q in reactions 8 and 19 (see Fig. 1). This competition results in a slower increase in the steady-state rate of respiration with decreasing $\Delta\Psi$ during oxidation of NADH + succinate (Fig. 4,E) compared to oxidation of NADH alone (Fig. 2,E). As a consequence, addition of succinate as the second respiratory substrate to NADH results in a slower decline of the total rate of superoxide production (Fig. 4,A) and at the site FMNH$^-$ (Fig. 4,B) with a decrease in $\Delta\Psi$, than is found during oxidation of NADH alone (Fig. 2,A and 2,B). Moreover, chronic ethanol-induced inhibition of the respiratory chain results in additional slowing down of the respiration rate and increasing the total rate of superoxide production (Fig. 4,A) and at the site FMNH$^-$ (Fig. 4,B). The rate of superoxide generation by the semiquinone of Complex I (Fig. 4,C) is not affected by chronic ethanol treatment during oxidation of NADH + succinate just as during oxidation of NADH alone (Fig. 2,C). By contrast, chronic ethanol exposure shifts the rate of superoxide generation by the unstable semiquinone of Complex III to a lower values of the membrane potential which results from slowing down in the rate respiration and, as a result, saturation of the respiration rate at a lower $\Delta\Psi$.

Besides, it should be pointed out that the maximal rate of respiration during oxidation of NADH + succinate (Fig. 4,E) becomes equal to the sum of the maximal respiration rates during oxidation of NADH alone (Fig. 2,E) and succinate alone (Fig. 3,E). However, it affects a little bit a relationship between the total rate of superoxide production and the respiration rate (Fig. 4,F).
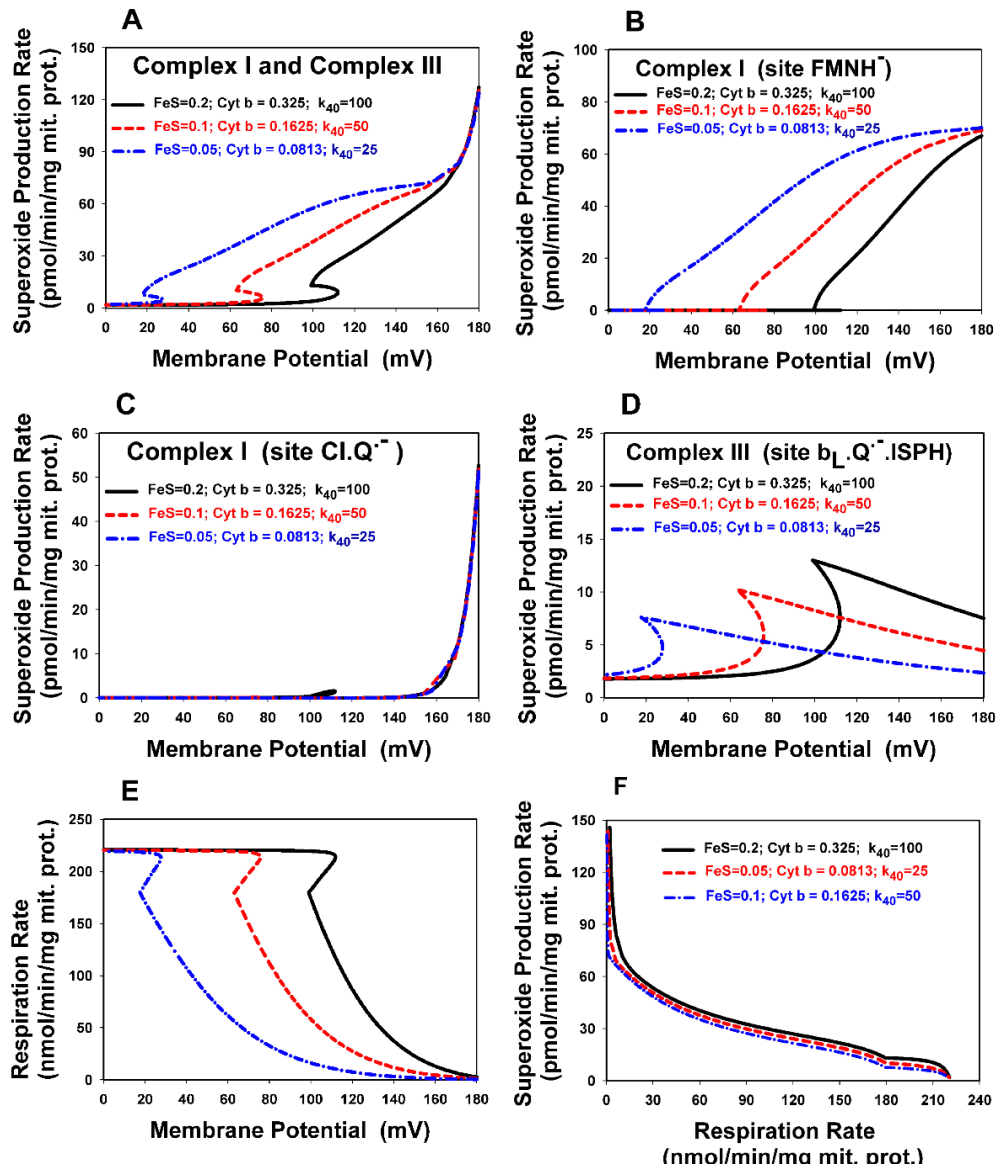
Figure 4. Computer simulated changes in the steady-state rates of respiration and superoxide production upon chronic ethanol-induced alterations in different segments of the respiratory chain during oxidation of NADH + succinate. Computer simulation was carried out with the mathematical model at kinetic parameter values presented in Table 2. Different curves (black solid, red dashed and blue dash-dot curves) correspond to different values of the levels of FeS redox centers in Complex I and cytochrome b in Complex III, and the catalytic rate constant, k_{40}, of cytochrome c oxidase. Black solid curves correspond to the control values – FeS = 0.2 nmol/ mg mit prot; cyt b = 0.325 nmol/ mg mit prot; k_{40} = 100 s^{-1}. Red dashed curves – FeS = 0.1 nmol/ mg mit prot; cyt b = 0.1625 nmol/ mg mit prot; k_{40} = 50 s^{-1}. Blue dash-dot curves – FeS = 0.05 nmol/ mg mit prot; cyt b = 0.0813 nmol/mg mit prot; k_{40} = 25 s^{-1}. Designation for every curve is also shown in Fig.4. (**A**) The total rate of superoxide production by Complexes I and III**.** (**B–D**) The rate of superoxide generation by different sites of Complexes I and III: (**B**) the site FMNH$^-$ of Complex I; (**C**) the semiquinone of Complex I (site CI.Q$^{\cdot-}$); (**D**) the unstable semiquinone of Complex III (site bL.Q$^{\cdot-}$.ISPH). (**E**) The steady-state respiration rate at different values of the membrane potential. (**F**) Relationships between rates of superoxide production and respiration. All these computer simulated results were obtained during oxidation of NADH + succinate, i.e. k_{15} = 0.3 s^{-1} and V_{max19} = 3000 µM/s.

Summarizing results in this section we may conclude that our computer simulated results account for chronic ethanol-related inhibition of the respiratory rate over the range of membrane potential of a $\Delta\Psi < 180$ mV during oxidation of different respiratory substrates observed experimentally in our laboratory [12]. Besides, computational results predict an increase in the total ROS production rate over the same range of membrane potential during oxidation of NADH alone and NADH + succinate. We predict that the effect of chronic

79

ethanol consumption on the total ROS production rate during oxidation of succinate alone depends on the membrane potential. Chronic ethanol consumption is expected to inhibit the ROS production rate during oxidation of succinate alone over the range of membrane potential of approximately $\Delta\Psi > 145$ mV. The ROS production rate is activated after chronic ethanol consumption at $\Delta\Psi < 145$ mV during oxidation of succinate alone.

2. Computer simulated changes in the steady-state mitochondrial concentration of superoxide and H_2O_2 upon chronic ethanol exposure

Changes in the mitochondrial ROS concentration upon chronic ethanol exposure depend on alterations in both the ROS generating respiratory chain and ROS utilizing glutathione cycle. We analyzed above the effect of chronic ethanol-induced inhibition of the respiratory chain on the rate of superoxide production during oxidation of different substrates. Now, we consider additionally the effect of experimentally observed chronic ethanol-induced alterations in the glutathione cycle [11, 16] on the mitochondrial ROS concentration during oxidation of different respiratory substrates.

Chronic ethanol-induced alterations in the glutathione cycle include a decrease in the mitochondrial glutathione peroxidase activity and an increase in the activity of glutathione reductase [11]. Besides, there are contradictory published data about the effect of chronic ethanol consumption on the mitochondrial glutathione levels. As experimental observations show the total glutathione levels in liver mitochondria can decrease [66, 67], increase [11] or remain unchanged [68] after chronic ethanol consumption. Analysis of our computational model shows that the 2-fold decrease or 2-fold increase in the total glutathione level only does not affect the steady-state concentration of superoxide and H_2O_2 in mitochondria (data are not shown). Therefore, we used in our computational modeling analysis the all set of experimental data published in [11] which include an increase in the total glutathione level in mitochondria. In accord with experimental observations [11], mitochondrial glutathione peroxidase (GSHPx–1) activity decreased approximately (30%) from 219 to 162 nmol NADPH oxidized /min/mg prot and glutathione reductase (GR) activities increased (10%) from 20 to 22 nmol NADPH oxidized /min/mg prot. upon chronic ethanol treatment. We approximated chronic ethanol-induced decrease (219/162 = 1.35) in the GSHPx–1 activity and an increase (22/20 = 1.1) in GR activity due to 1.35-fold decrease in mitochondrial GSHPx-1 concentration [E_{tot}] from 1.77 μM (Table 2) to 1.31 μM and 1.1-fold increase in the maximal rate (V_{max42}) of GR from 1 μM/s to 1.1 μM/s. Besides, the mitochondrial glutathione level was increased (25%) from 10 to 12.5 nmol/mg prot. upon chronic ethanol exposure [11], i.e. from 4222 (Table 2) to 5278 μM in our computations.

Computer simulated changes in the steady-state concentration of superoxide and H_2O_2 in the mitochondrial matrix and IMS upon chronic ethanol-induced alterations in different segments of the respiratory chain and glutathione cycle during oxidation of different respiratory substrates are presented in Fig. 5–7. In order to better understand the effect of different alterations on the ROS concentration, Fig. 5–7 present separately ROS concentration under control condition which correspond to control parameter values presented in Table 2 (black solid curves), under chronic ethanol-induced alterations in the respiratory chain only (red dashed curves), only glutathione cycle (blue dash-dot curves), and simultaneous alterations in the respiratory chain and glutathione cycle (green dash-dot-dot curves).

Fig. 5 presents computer simulated chronic ethanol-induced changes in the steady-state concentration of superoxide in the mitochondrial matrix (Fig. 5,A) and IMS (Fig. 5,B), and the H_2O_2 concentration in the mitochondrial matrix (Fig. 5,C) and IMS (Fig. 5,D) during oxidation of NADH alone. First of all, it should be pointed out that the experimentally observed steady-state concentration of superoxide and H_2O_2 in rat liver mitochondria that equal to 0.083 nM and 4.8 nM, respectively, [17] is very close to those obtained computationally in the mitochondrial matrix at $\Delta\Psi \approx 170$ mV under control condition (black

solid curves in Fig. 5,A and 5,C). The overall computer simulated steady-state concentration of superoxide and H_2O_2 in mitochondria will be a little higher due to taking into account higher values of the steady-state concentration of superoxide and H_2O_2 in the IMS (Fig. 5,B and 5,D).
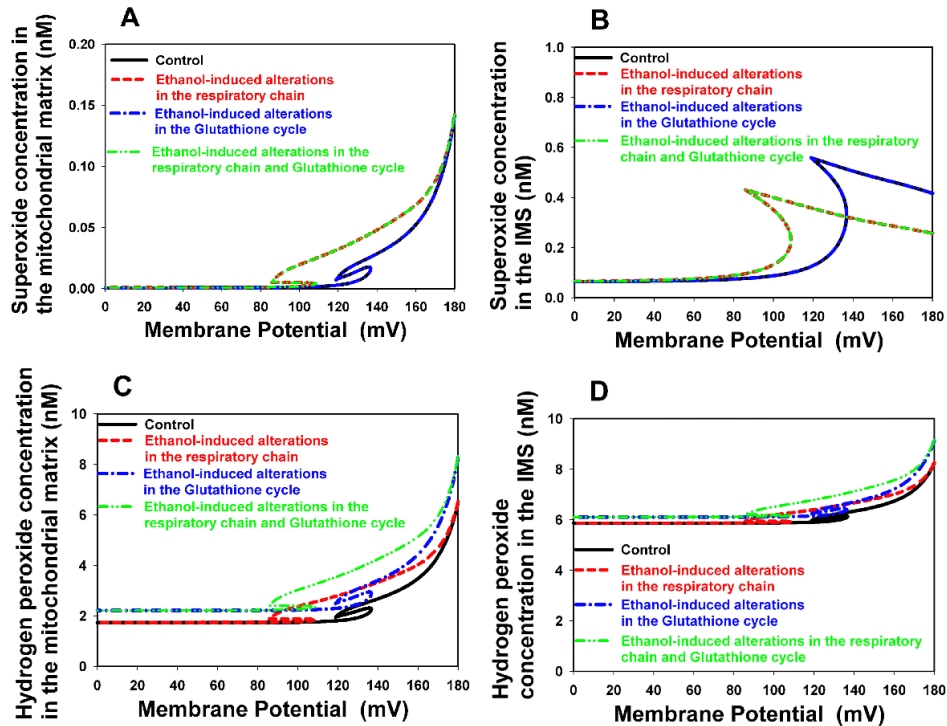

Figure 5. Computer simulated changes in the steady-state concentration of superoxide and H_2O_2 in the mitochondrial matrix and IMS upon chronic ethanol-induced alterations in different segments of the respiratory chain and glutathione cycle during oxidation of NADH alone. Different curves (black solid, red dashed, blue dash-dot, and green dash-dot-dot curves) correspond to different chronic ethanol-induced alterations in the respiratory chain and glutathione cycle. Alterations in the respiratory chain include simultaneous changes in values of the levels of FeS redox centers in Complex I and cytochrome b in Complex III, and the catalytic rate constant, k_{40}, of cytochrome c oxidase. Chronic ethanol-induced alterations in the glutathione cycle include a decrease in the mitochondrial glutathione peroxidase concentration, $[GPx]_{tot}$, an increase in the maximal rate of glutathione reductase reaction, V_{max42}, and an increase in the mitochondrial glutathione concentration, $[G]_{tot}$. Black solid curves correspond to the control values of the model parameters which are presented in Table 2 and have the following values for the glutathione cycle: $[GPx]_{tot} = 1.77$ μM, $V_{max42}=1$ μM/s, and $[G]_{tot} = 4222$ μM. Red dashed curves correspond to alterations only in the respiratory chain – FeS = 0.1 nmol/ mg mit prot; cyt b = 0.1625 nmol/ mg mit prot; $k_{40} = 50$ s⁻¹. Blue dash-dot curves correspond to alterations only in the glutathione cycle – $[GPx]_{tot} = 1.31$ μM, $V_{max42} = 1.1$ μM/s, and $[G]_{tot} = 5278$ μM. Green dash-dot-dot curves correspond to simultaneous alterations in the respiratory chain and glutathione cycle – FeS = 0.1 nmol/ mg mit prot; cyt b = 0.1625 nmol/ mg mit prot; $k_{40} = 50$ s⁻¹; $[GPx]_{tot} = 1.31$ μM, $V_{max42} = 1.1$ μM/s, and $[G]_{tot} = 5278$ μM. Designations for every curve are also shown in Fig. 5. (**A, B**) The concentration of superoxide in the mitochondrial matrix (A) and IMS (B). (**C, D**) The concentration of H_2O_2 in the mitochondrial matrix (C) and IMS (D). All these computer simulated results were obtained during oxidation of NADH alone, i.e. $k_{15} = 0.3$ s⁻¹ and $V_{max19} = 0$. Other kinetic parameter values are presented in Table 2.

A ΔΨ dependency of the concentration of superoxide in the mitochondrial matrix (Fig. 5,A) and IMS (Fig. 5,B) resembles ΔΨ dependency of the total rate of superoxide production (Fig. 2,A) and the rate of superoxide generation by the unstable semiquinone of Complex III (Fig. 2,D), respectively. This is an expected result because a degradation of superoxide does not dependent on the membrane potential in the computational model. As to the effect of chronic ethanol-induced alterations in the respiratory chain and glutathione cycle on the ROS concentration, we should point out the following. The concentration of

81

superoxide in the mitochondrial matrix (Fig. 5,A) and IMS (Fig. 5,B) is affected by alterations in the respiratory chain only while H_2O_2 concentration (Fig. 5,C and 5,D) increases upon alterations in both the respiratory chain and glutathione cycle during oxidation of NADH alone. Independence of the superoxide concentration on alterations in the glutathione cycle is accounted for by irreversible dismutation of superoxide to H_2O_2 in the mitochondrial matrix (reaction 18) and IMS (reaction 30 in Fig. 1 and Table 1).
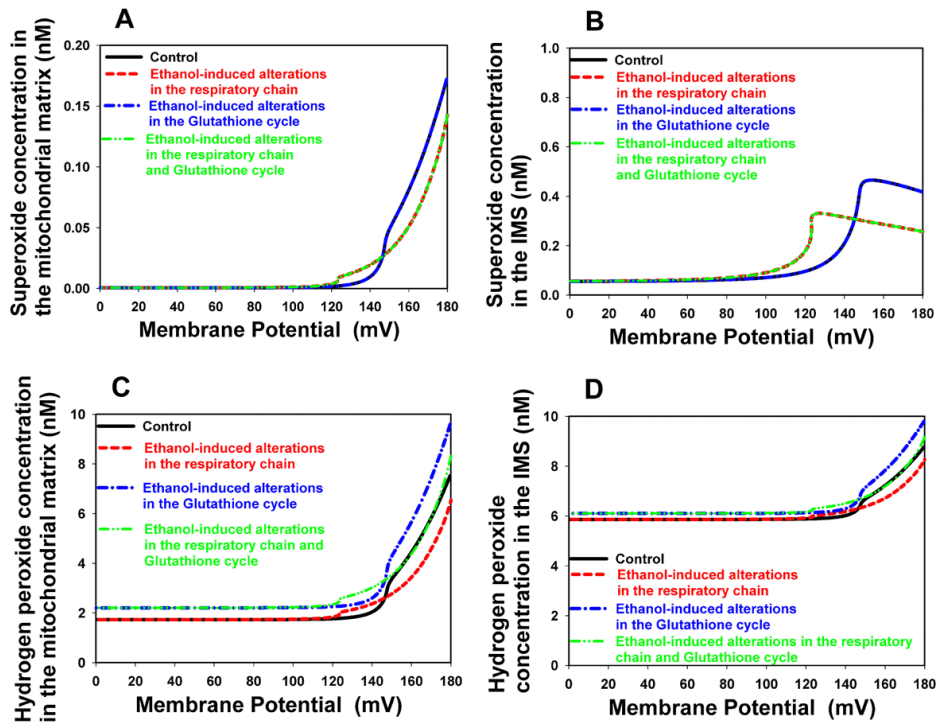

Figure 6. Computer simulated changes in the steady-state concentration of superoxide and H_2O_2 in the mitochondrial matrix and IMS upon chronic ethanol-induced alterations in different segments of the respiratory chain and glutathione cycle during oxidation of succinate alone. Different curves (black solid, red dashed, blue dash-dot, and green dash-dot-dot curves) correspond to different chronic ethanol-induced alterations in the respiratory chain and glutathione cycle. Alterations in the respiratory chain include simultaneous changes in values of the levels of FeS redox centers in Complex I and cytochrome b in Complex III, and the catalytic rate constant, k_{40}, of cytochrome c oxidase. Chronic ethanol-induced alterations in the glutathione cycle include a decrease in the mitochondrial glutathione peroxidase concentration, $[GPx]_{tot}$, an increase in the maximal rate of glutathione reductase reaction, V_{max42}, and an increase in the mitochondrial glutathione concentration, $[G]_{tot}$. Black solid curves correspond to the control values of the model parameters which are presented in Table 2 and have the following values for the glutathione cycle: $[GPx]_{tot} = 1.77$ μM, $V_{max42} = 1$ μM/s, and $[G]_{tot} = 4222$ μM. Red dashed curves correspond to alterations only in the respiratory chain – FeS=0.1 nmol/ mg mit prot; cyt b = 0.1625 nmol/ mg mit prot; $k_{40} = 50$ s⁻¹. Blue dash-dot curves correspond to alterations only in the glutathione cycle – $[GPx]_{tot} = 1.31$ μM, $V_{max42} = 1.1$ μM/s, and $[G]_{tot} = 5278$ μM. Green dash-dot-dot curves correspond to simultaneous alterations in the respiratory chain and glutathione cycle – FeS = 0.1 nmol/ mg mit prot; cyt b = 0.1625 nmol/ mg mit prot; $k_{40} = 50$ s⁻¹; $[GPx]_{tot} = 1.31$ μM, $V_{max42} = 1.1$ μM/s, and $[G]_{tot} = 5278$ μM. Designations for every curve are also shown in Fig. 6. (**A, B**) The concentration of superoxide in the mitochondrial matrix (A) and IMS (B). (**C, D**) The concentration of H_2O_2 in the mitochondrial matrix (C) and IMS (D). All these computer simulated results were obtained during oxidation of NADH alone, i.e. $k_{15} = 0$ and $V_{max19} = 3000$ μM/s. Other kinetic parameter values are presented in Table 2.

The computer simulated effects of ethanol-induced alterations in both the respiratory chain and glutathione cycle on the ROS concentration in the mitochondrial matrix and IMS during oxidation of succinate alone are presented in Fig. 6,A–D. Likewise during oxidation of NADH alone, the concentration of superoxide in the mitochondrial matrix (Fig. 6,A) and IMS (Fig. 6,B) is affected by alterations in the respiratory chain only while H_2O_2 concentration

(Fig. 6,C and 6,D) changes upon alterations in both the respiratory chain and glutathione cycle during oxidation of succinate alone. However, in contrast to oxidation of NADH alone, the ethanol-induced effect on the concentration of $O_2^{\bullet-}$ in the mitochondrial matrix and IMS is non-monotonic and depends on the membrane potential just as in the case of the total rate of superoxide production (Fig. 3,A) and by the unstable semiquinone of Complex III (Fig. 3,D) during oxidation of succinate alone.
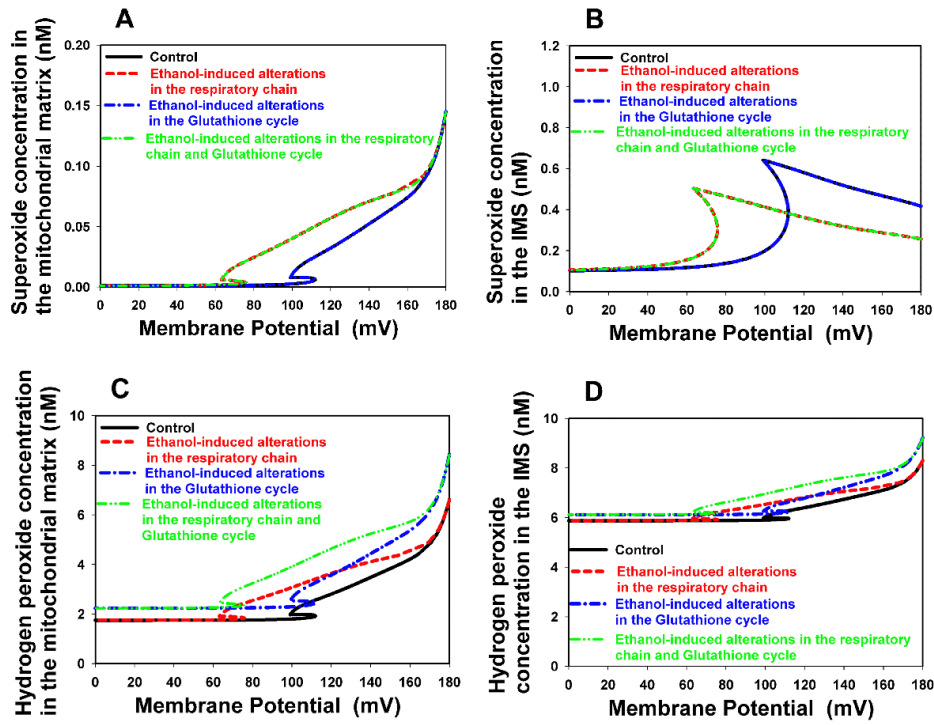

Figure 7. Computer simulated changes in the steady-state concentration of superoxide and H_2O_2 in the mitochondrial matrix and IMS upon chronic ethanol-induced alterations in different segments of the respiratory chain and glutathione cycle during oxidation of NADH + succinate. Different curves (black solid, red dashed, blue dash-dot, and green dash-dot-dot curves) correspond to different chronic ethanol-induced alterations in the respiratory chain and glutathione cycle. Alterations in the respiratory chain include simultaneous changes in values of the levels of FeS redox centers in Complex I and cytochrome b in Complex III, and the catalytic rate constant, k_{40}, of cytochrome c oxidase. Chronic ethanol-induced alterations in the glutathione cycle include a decrease in the mitochondrial glutathione peroxidase concentration, $[GPx]_{tot}$, an increase in the maximal rate of glutathione reductase reaction, V_{max42}, and an increase in the mitochondrial glutathione concentration, $[G]_{tot}$. Black solid curves correspond to the control values of the model parameters which are presented in Table 2 and have the following parameter values for the glutathione cycle: $[GPx]_{tot} = 1.77$ μM, $V_{max42} = 1$ μM/s, and $[G]_{tot} = 4222$ μM. Red dashed curves correspond to alterations only in the respiratory chain – FeS = 0.1 nmol/ mg mit prot; cyt b = 0.1625 nmol/ mg mit prot; $k_{40} = 50$ s⁻¹. Blue dash-dot curves correspond to alterations only in the glutathione cycle – $[GPx]_{tot} = 1.31$ μM, $V_{max42} = 1.1$ μM/s, and $[G]_{tot} = 5278$ μM. Green dash-dot-dot curves correspond to simultaneous alterations in the respiratory chain and glutathione cycle – FeS = 0.1 nmol/ mg mit prot; cyt b = 0.1625 nmol/ mg mit prot; $k_{40} = 50$ s⁻¹; $[GPx]_{tot} = 1.31$ μM, $V_{max42} = 1.1$ μM/s, and $[G]_{tot} = 5278$ μM. Designations for every curve are also shown in Fig. 7. (**A, B**) The concentration of superoxide in the mitochondrial matrix (A) and IMS (B). (**C, D**) The concentration of H_2O_2 in the mitochondrial matrix (C) and IMS (D). All these computer simulated results were obtained during oxidation of NADH + succinate, i.e. $k_{15} = 0.3$ s⁻¹ and $V_{max19} = 3000$ μM/s. Other kinetic parameter values are presented in Table 2.

The superoxide concentration as well as the rate of superoxide production increases over the entire range of membrane potential below a $\Delta\Psi$ of approximately 145 mV and it decreases at $\Delta\Psi > 145$ mV upon chronic ethanol-induced inhibition of Complexes I, III and IV. The concentration of H_2O_2 in the mitochondrial matrix and IMS upon inhibition of the respiratory chain only (dashed red curves in Fig. 6,C and 6,D) follows the superoxide concentration and

is also non-monotonic and depends on the membrane potential. However, the concentration of H_2O_2 increases over the entire range of membrane potential of a $\Delta\Psi < 180$ mV upon alterations in the glutathione cycle during oxidation of succinate alone (Fig. 6,C and 6,D).

Fig. 7 shows that the effect of chronic ethanol-induced alterations in both the respiratory chain and glutathione cycle on the concentration of superoxide and H_2O_2 in the mitochondrial matrix and IMS during oxidation of NADH + succinate is very similar to that observed during oxidation of NADH alone (Fig. 5). There is only a difference between them that the ROS concentration during oxidation of NADH + succinate is a little higher than during oxidation of NADH alone. These computer simulated chronic ethanol-induced increase in the mitochondrial ROS concentration during oxidation of NADH + succinate are compatible with the increased level of ROS in isolated hepatocytes from ethanol-fed rats compared to the control rats [7].

3. Computer simulation of the effects of acute ethanol consumption on ROS production

One of the consequences of acute ethanol consumption which affects ROS production by the respiratory chain is a shift in the intracellular redox state due to generation of excess of cytosolic NADH during oxidation of ethanol by alcohol dehydrogenase [5, 69]. Ethanol-induced excess of cytosolic NADH results in an increase in the mitochondrial NADH/NAD$^+$ ratio depending on malate-aspartate shuttle in the inner mitochondrial membrane [8] and a considerable increase in the rate of ROS generation in the respiratory chain [6, 7]. Besides, an increase in the mitochondrial NADH/NAD$^+$ ratio can considerably increase the rate of ROS production by α-ketoglutarate dehydrogenase [70] which is also an important mitochondrial source of ROS as was demonstrated in isolated brain mitochondria [71].
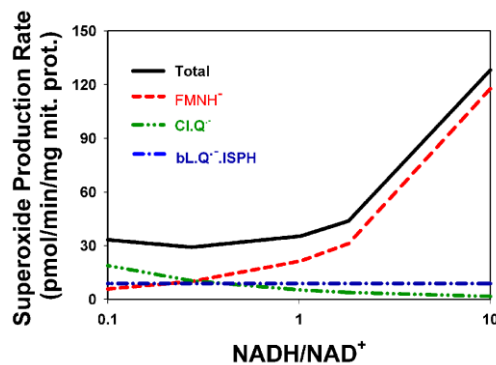

Figure 8. Computer simulated changes in the steady-state rates of superoxide production at different sites of the respiratory chain upon acute ethanol-induced alterations in NADH/NAD$^+$ ratio during oxidation of NADH + succinate. Different curves (black solid, red dashed, blue dash-dot, and green dash-dot-dot curve) correspond to different sites of superoxide formation in the respiratory chain. Black solid curve is the total rate of superoxide production by Complexes I and III; red dashed curve is the rate of superoxide generation by the FMNH$^-$ of Complex I; blue dash-dot curve – by the semiquinone of Complex I (site CI.Q$^-$); green dash-dot-dot curve – by the unstable semiquinone of Complex III (site b$_L$.Q$^-$.ISPH). Designation for every curve is also shown in Fig. 8. Computer simulation was carried out with the mathematical model at kinetic parameter values presented in Table 2, exclude $K_{eq15} = 50$ and k_{15} which was varied in order to keep different steady-state values of NADH/NAD$^+$ ratio presented in Fig. 8. at $\Delta\Psi = 165$ mV. It should note that NADH and NAD$^+$ in the ratio NADH/NAD$^+$ are total, free and bound to FMN, concentration of NADH and NAD$^+$, respectively, i.e. [NADH]$_{total}$ = [NADH] + [FMN.NADH] + [FMNH$^-$.NADH]; [NAD$^+$]$_{total}$ = NAD$^+$ + [FMN.NAD$^+$] + [FMNH$^-$.NAD$^+$]. Computer simulated results were obtained during oxidation of NADH + succinate, i.e. $k_{15} = 0.3$ s^{-1} and $V_{max19} = 3000$ μM/s.

In this work, we analyzed computationally the effect of variation in the mitochondrial NADH/NAD$^+$ ratio on ROS production by the respiratory chain only. Although, the mitochondrial NADH/NAD$^+$ ratio in intact cells varies from 0.1 to 1 [72] we considered changes in this ratio from 0.1 to 10 in our computational study in order to take into account

additional generation of NADH due to ethanol oxidation. Fig. 8 presents alterations in the rate of superoxide production by different sites of the respiratory chain during acute ethanol-induced increase in the value of NADH/NAD$^+$ ratio from 0.1 to 10. As Fig. 8 shows the total rate of superoxide production (black solid curve) as well as the rate of superoxide generation by the site FMNH$^-$ (red dashed curve) increases with increasing the NADH/NAD$^+$ ratio. However, the rate of superoxide generation by the semiquinone of Complex I decreases and by the unstable semiquinone of Complex III is not changed with increasing the NADH/NAD$^+$ ratio. An increase in the rate of superoxide generation by the FMNH$^-$ with increasing the NADH/NAD$^+$ ratio is clear and accounted for by increasing FMNH$^-$ with increasing of reduced NADH.
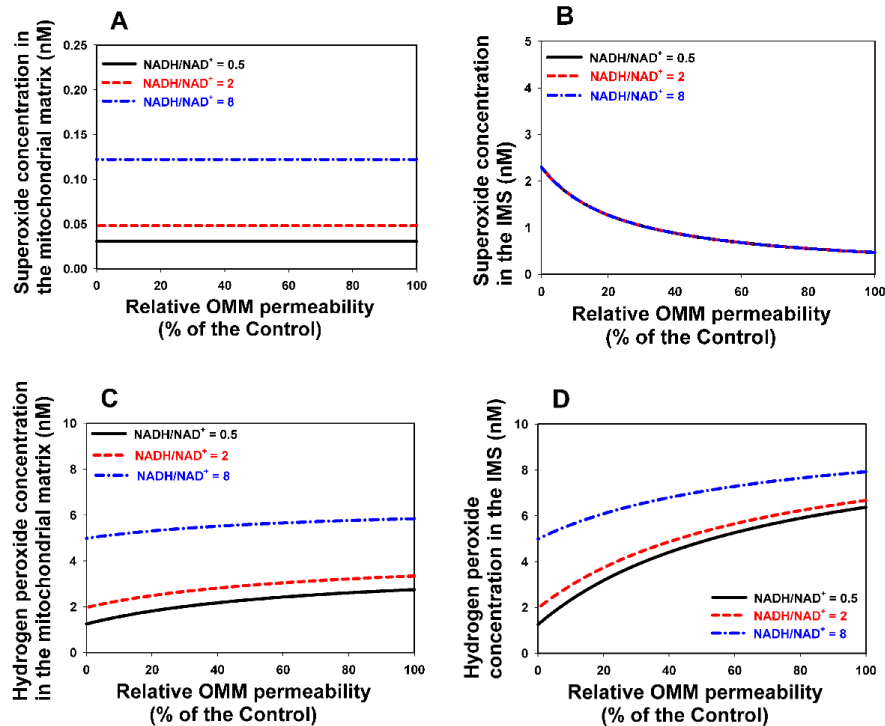

Figure 9. Computer simulated changes in the steady-state concentration of superoxide and H$_2$O$_2$ in the mitochondrial matrix and IMS upon acute ethanol-induced alterations in the outer mitochondrial membrane permeability and NADH/NAD$^+$ ratio. Figs. (**A–D**) present changes in the concentration of superoxide anion and hydrogen peroxide in the mitochondrial matrix, (**A**) and (**C**), and in the intermembrane space (IMS), (**B**) and (**D**), with changing relative OMM permeability for O$_2^{\bullet-}$ and H$_2$O$_2$ at different values of NADH/NAD$^+$ ratio. Black solid curves in all Figs correspond to NADH/NAD$^+$ = 0.5; red dashed curves – NADH/NAD$^+$ = 2; blue dash-dot curves – NADH/NAD$^+$ = 8. Designation for every curve is also shown in Fig. 10. Simulation of decreasing OMM permeability was made computationally as follows. A coefficient $\alpha = P_{curr}/P_{cntr}$, where P_{curr} and P_{cntr} are the current and control OMM permeability, respectively, was introduced in order to describe current relative OMM permeability which, if measured in %, equals to 100·α. In this case, current values of the rate constants of transport of H$_2$O$_2$ and superoxide through OMM were taken as $\alpha \cdot k_{44}$ and $\alpha \cdot k_{45}$, where control values k_{44} = 30 s^{-1} and k_{45} = 500 s^{-1} (Table 2). Values of NADH/NAD$^+$ ratio were adjusted by variation in value of the rate constant k_{15} at K_{eq15} = 10 and $\Delta\Psi$ = 160 mV. NADH/NAD$^+$ = 0.5 corresponds to k_{15} = 0.024 s^{-1}; NADH/NAD$^+$ = 2 corresponds to k_{15} = 0.055 s^{-1}; NADH/NAD$^+$ = 8 corresponds to k_{15} = 0.57 s^{-1}. All presented computer simulated results were obtained at $\Delta\Psi$ = 160 mV during oxidation of NADH + succinate, i.e. V_{max19} = 3000 μM/s and values of k_{15} pointed above. Other kinetic parameter values are presented in Table 2.

However, computational study shows that the rate of respiration changes very little with increasing the NADH/NAD$^+$ ratio from 0.1 to 10 at $\Delta\Psi$ = 165 mV (data are not shown). As a result the rate of superoxide generation by the unstable semiquinone of Complex III is not changed and ROS production by the semiquinone of Complex I decreases slowly with increasing the NADH/NAD$^+$ ratio from 0.1 to 10. It should be pointed out that these computer

simulated results are compatible with experimental observations of ROS production in freshly isolated hepatocytes during acute ethanol metabolism [6, 7]. Treatment of hepatocytes with 1 and 10 mM ethanol led to a dose-related increase in ROS production by 72 and 151 %, respectively, [6] just as with increasing the NADH/NAD$^+$ ratio up to approximately of 2 and 4 in our computer simulations.

Fig. 9 presents changes in the concentration of superoxide anion and hydrogen peroxide in the mitochondrial matrix, (Fig. 9,A) and (Fig. 9,C), and in the intermembrane space (IMS), (Fig. 9,B) and (Fig. 9,D), with changing relative OMM permeability for superoxide and H_2O_2 at different values of NADH/NAD$^+$ ratio. The concentration of superoxide in IMS increases considerably upon ethanol-induced decrease in the OMM permeability due to very low values of superoxide in the cytoplasm, which is around $2.5 \cdot 10^{-11}$ M [46]. By contrast, the concentration of H_2O_2 decreases in the both IMS and mitochondrial matrix with decreasing the OMM permeability because of a high concentration of H_2O_2 in the cytoplasm, which is around 10 nM [46].

CONCLUSION

A computational mechanistic model of electron transfer and superoxide formation in the mitochondrial respiratory chain was developed in the current work. The model takes into account also reactions of formation and degradation of mitochondrial hydrogen peroxide catalyzed by Superoxide anion dismutatase (Mn-SOD), Glutathione peroxidase and reductase. The computational model consists of 35 ordinary differential equations (ODE) and 14 moiety conservation equations. The control, acute and chronic alcohol consumption were simulated with the help of the model to account for available experimental data on ROS production under different physiological conditions. Computational analysis shows very good quantitative coincidence experimental and computer simulated results under control condition and predicts a $\Delta\Psi$-dependent effect of acute and chronic ethanol on mitochondrial ROS production which can be tested experimentally.

Acknowlegdements

REFERENCES

1. Bailey S.M., Cunningham C.C. *Free Radic. Biol. Med.* 2002. V. 32. P. 11–16.
2. Cahill A., Cunningham C.C., Adachi M., Ishii H., Bailey S.M., Fromenty B., Davies A. *Alcohol. Clin. Exp. Res.* 2002. V. 26. P. 907–915.
3. Cederbaum A.I., Lu Y., Wu D. *Arch. Toxicol.* 2009. V. 83. P. 519–548.
4. Muller F.L., Liu Y., Van Remmen H. *J. Biol. Chem.* 2004. V. 279. P. 49064–49073.
5. Cunningham C.C., Malloy C.R., Radda G.K. *Biochim. Biophys. Acta.* 1986. V. 885. P. 12–22.
6. Bailey S.M., Pietsch E.C., Cunningham C.C. *Free Radic. Biol. Med.* 1999. V. 27. P. 891–900.
7. Bailey S.M., Cunningham C.C. *Hepatology* 1998. V. 28. P. 1318–1326.
8. Sugano T., Handler J.A., Yoshihara H., Kizaki Z., Thurman R.G. *J. Biol. Chem.* 1990. V. 265. P. 21549–21553.
9. Tikunov A., Johnson C.B., Pediaditakis P., Markevich N., Macdonald J.M., Lemasters J.J., Holmuhamedov E. *Arch. Biochem. Biophys.* 2010. V. 495. P. 174–181.
10. Hirano T., Kaplowitz N., Tsukamoto H., Kamimura S., Fernandez-Checa J.C. *Hepatology.* 1992. V. 16. P. 1423–1427.
11. Bailey S.M., Patel V.B., Young T.A., Asayama K., Cunningham C.C. *Alcohol. Clin. Exp. Res.* 2001. V. 25. P. 726–733.

12. Marcinkeviciute A., Mildaziene V., Crumm S., Demin O., Hoek J.B., Kholodenko B. *Biochem. J.* 2000. V. 349. P. 519–526.
13. Thayer W.S., Ohnishi T., Rubin E. *Biochim. Biophys. Acta.* 1980. V. 591. P. 22–36.
14. Thayer W.S., Rubin E. *J. Biol. Chem.* 1981. V. 256. P. 6090–6097.
15. Piquet M.A., Nogueira V., Devin A., Sibille B., Filippi C., Fontaine E., Roulet M., Rigoulet M., Leverve X.M. *FEBS Lett.* 2000. V. 468. P. 239–242.
16. Fernandez-Checa J.C., Kaplowitz N., Colell A., Garcia-Ruiz C. *Alcohol. Health. Res. World.* 1997. V. 21. P. 321–324.
17. Cadenas E., Boveris A. *Biochem. J.* 1980. V. 188. P. 31–37.
18. Demin O.V., Kholodenko B.N., Skulachev V.P. *Mol. Cell. Biochem.* 1998. V. 184. P. 21–33.
19. Grivennikova V.G., Vinogradov A.D. *Biochim. Biophys. Acta.* 1982. V. 682. P. 491–495.
20. Beard D.A. *PLoS Comput. Biol.* 2005. V. 1. P. e36.
21. Toppo S., Flohe L., Ursini F., Vanin S., Maiorino M. *Biochim. Biophys. Acta.* 2009. V. 1790. 1486–1500.
22. Carlberg I., Mannervik B. *J. Biol. Chem.* 1975. V. 250. P. 5475–5480.
23. Grivennikova V.G., Kotlyar A.B., Karliner J.S., Cecchini G., Vinogradov A.D. *Biochemistry* 2007. V. 46. P. 10971–10978.
24. Verkhovskaya M.L., Belevich N., Euro L., Wikstrom M., Verkhovsky M.I. *Proc. Natl. Acad. Sci. U S A* 2008. V. 105. P. 3763–3767.
25. Ransac S., Arnarez C., Mazat J.P. *Biochim. Biophys. Acta.* 2011. V. 1797. P. 641–648.
26. Kussmaul L., Hirst J. *Proc. Natl. Acad. Sci. U S A* 2006 V. 103. P. 7607–7612.
27. Brandt U. *Annu. Rev. Biochem.* 2006. V. 75. P. 69–92.
28. Ohnishi T. *Biochim. Biophys. Acta.* 1998. V. 1364. P. 186–206.
29. Moser C.C., Farid T.A., Chobot S.E., Dutton P.L. *Biochim. Biophys. Acta.* 2006. V. 1757. P. 1096–1109.
30. Murphy M.P. *Biochem. J.* 2009. V. 417. P. 1–13.
31. Hsu J.L., Hsieh Y., Tu C., O'Connor D., Nick H.S., Silverman D.N. *J. Biol. Chem.* 1996. V. 271. P. 17687–17691.
32. Tyler D.D. *Biochem. J.* 1975. V. 147. P. 493–504.
33. Crofts A.R., Lhee S., Crofts S.B., Cheng J., Rose S. *Biochim. Biophys. Acta.* 2006. V. 1757. P. 1019–1034.
34. Shinkarev V.P., Wraight C.A. *FEBS Lett.* 2007. V. 581. P. 1535–1541.
35. Crofts A.R., Shinkarev V.P., Kolling D.R., Hong S. *J. Biol. Chem.* 2003. V. 278. P. 36191–36201.
36. Bielski B.H., Cabelli D.E. *Int. J. Radiat. Biol.* 1991. V. 59. P. 291–319.
37. Battistuzzi G., Borsari M., Cowan J.A., Ranieri A., Sola M. *J. Am. Chem. Soc.* 2002. V. 124. P. 5315–5124.
38. Butler J., Jayson G.G., Swallow A.J. *Biochim. Biophys. Acta.* 1975. V. 408. P. 215–222.
39. Butler J., Koppenol W.H., Margoliash E. *J. Biol. Chem.* 1982. V. 257. P. 10747–10750.
40. Covian R., Trumpower B.L. *Biochim. Biophys. Acta.* 2008. V. 1777. P. 1044–1052.
41. Engstrom G., Rajagukguk R., Saunders A.J., Patel C.N., Rajagukguk S., Merbitz-Zahradnik T., Xiao K., Pielak G.J., Trumpower B., Yu C.A., Yu L., Durham B., Millett F. *Biochemistry.* 2003. V. 42. P. 2816–2824.
42. Millett F., Durham B. *Photosynth. Res.* 2004. V. 82. P. 1–16.
43. Takebe G., Yarimizu J., Saito Y., Hayashi T., Nakamura H., Yodoi J., Nagasawa S., Takahashi K. *J. Biol. Chem.* 2002. V. 277. P. 41254–41258.
44. Ulusu N.N., Tandogan B. *Mol. Cell. Biochem.* 2007. V. 303. P. 45–51.
45. Mailloux R.J., Harper M.E. *Faseb. J.* 2011. V. 24. P. 2495–2506.
46. Boveris A. *Medicina (B Aires).* 1998. V. 58. P. 350–356.

47. Tamura T., McMicken H.W., Smith C.V., Hansen T.N. *Biochem. Biophys. Res. Commun.* 1996. V. 222. P. 659–663.
48. Calamita G., Gena P., Meleleo D., Ferri D., Svelto M. *Biochim. Biophys. Acta.* 2006. V. 1758. P. 1018–1024.
49. Vinogradov A.D. *Biochim. Biophys. Acta*. 1998. V. 1364. P. 169–185.
50. Lambert A.J., Buckingham J.A., Boysen H.M., Brand M.D. *Aging Cell.* 2011. V. 9. P. 78–91.
51. Hackenbrock C.R., Chazotte B., Gupte S.S. *J. Bioenerg. Biomembr.* 1986. V. 18. P. 331–368.
52. Vinogradov A.D. *Biochim. Biophys. Acta*. 2008. V. 1777. P. 729–734.
53. Efremov R.G., Baradaran R., Sazanov L.A. *Nature*. 2010. V. 465. P. 441–445.
54. Vinogradov A.D., Sled V.D., Burbaev D.S., Grivennikova V.G., Moroz I.A., Ohnishi T. *FEBS Lett.* 1995. V. 370. P. 83–87.
55. Magnitsky S., Toulokhonova L., Yano T., Sled V.D., Hagerhall C., Grivennikova V.G., Burbaev D.S., Vinogradov A.D., Ohnishi T. *J. Bioenerg. Biomembr.* 2002. V. 34. P. 193–208.
56. Kao M.C., Nakamaru-Ogiso E., Matsuno-Yagi A., Yagi T. *Biochemistry*. 2005. V. 44. P. 9545–9554.
57. Hirst J., King M.S., Pryde K.R. *Biochem. Soc. Trans.* 2008. V. 36. P. 976–980.
58. Mitchell P. *FEBS Lett*. 1975. V. 56. P. 1–6.
59. Crofts A.R., Barquera B., Gennis R.B., Kuras R., Guergova-Kuras M., Berry E.A. *Biochemistry.* 1999. V. 38. P. 15807–15826.
60. Yu C.A., Cen X., Ma H.W., Yin Y., Yu L., Esser L., Xia D. *Biochim. Biophys. Acta.* 2008. V. 1777. P. 1038–1043.
61. Cape J.L., Bowman M.K., Kramer D.M. *Proc. Natl. Acad. Sci. U S A.* 2007. V. 104. P. 7887–7892.
62. Vinnakota K.C., Bassingthwaighte J.B. *Am. J. Physiol. Heart. Circ. Physiol.* 2004. V. 286. P. H1742–H1749.
63. Wu F., Yang F., Vinnakota K.C., Beard D.A. *J. Biol. Chem.* 2007. V. 282. P. 24525–24537.
64. Schwerzmann K., Cruz-Orive L.M., Eggman R., Sanger A., Weibel E.R. *J. Cell. Biol.* 1986. V. 102. P. 97–103.
65. Selivanov V.A., Votyakova T.V., Zeak J.A., Trucco M., Roca J., Cascante M. *PLoS Comput. Biol.* 2009. V. 5. P. e1000619.
66. Fernandez-Checa J.C., Ookhtens M., Kaplowitz N. *J. Clin. Invest.* 1989. V. 83. P. 1247–1252.
67. Fernandez-Checa J.C., Garcia-Ruiz C., Ookhtens M., Kaplowitz N. *J. Clin. Invest.* 1991. V. 87. P. 397–405.
68. Deaciuc I.V., Fortunato F., D'Souza N.B., Hill D.B., Schmidt J., Lee E.Y., McClain C.J. *Alcohol. Clin. Exp. Res.* 1999. V. 23. P. 349–356.
69. Volpi E., Lucidi P., Cruciani G., Monacchia F., Reboldi G., Brunetti P., Bolli G.B., De Feo P. *J. Nutr.* 1997. V. 127. P. 2199–2204.
70. Tretter L., Adam-Vizi V. *J. Neurosci.* 2004. V. 24. P. 7771–7778.
71. Starkov A.A., Fiskum G., Chinopoulos C., Lorenzo B.J., Browne S.E., Patel M.S., Beal M.F. *J. Neurosci.* 2004. V. 24. P. 7779–7788.
72. Hoek J.B., Rydstrom J. *Biochem. J.* 1988. V. 254. P. 1–10.